Combustion and Flame

Oxidation kinetic of soot generated from ammonia-acetylene laminar diffusion flame

--Manuscript Draft--

Manuscript Number:	CNF-D-25-01346R2
Article Type:	Full Length Article
Keywords:	Ammonia; Soot; Functional groups; oxidation; Reaction kinetics
Corresponding Author:	Chenyang Fan, Ph.D Henan University of Science and Technology CHINA
First Author:	Shuainan Yang
Order of Authors:	Shuainan Yang
	Chenyang Fan, Ph.D
	Zheng Fu
	Ye Liu
	Huiyong Du
	Bin Xu
	Yidu Tong
	Mingliang Wei
Abstract:	Co-combustion of ammonia with hydrocarbon fuels and its effect on soot emission characteristics have garnered interest. In this study, the oxidation kinetics of soot generated in a laminar co-flow acetylene diffusion flame were investigated under 30–800 °C temperature-programmed oxidation and isothermal oxidation at 500°C, 600°C, and 700°C using thermogravimetric analysis (TGA). The evolution of functional groups on soot surfaces and gaseous products were monitored by Fourier transform infrared spectroscopy (FT-IR) and thermogravimetric analysis coupled with infrared spectroscopy (TG-IR), respectively. Results indicate that the activation energy for soot oxidation increases with higher NH3 substitution ratios (XNH3) and elevated temperatures. Isothermal oxidation tests also show that the oxidation rate constant increases with increasing XNH3. FTIR results show that increasing XNH3 reduces aliphatic C–H groups and increases oxygenated groups on soot surfaces. The detected C–N bonds are attributed to dehydrogenation of aliphatic carbon atoms on polycyclic aromatic hydrocarbons (PAHs) surfaces. TG-IR analysis revealed the C–N bonds in urethanes on soot surfaces may release as the gaseous C–N species during low-temperature (500 °C) oxidation of soot particles. Nevertheless, the higher-temperature facilitated the cleavage of C–N bonds, and then the generated NH2 radicals react with oxygen radicals, leading to the formation of HNO on the soot surface.

Declaration of interests

☒ The authors declare that they have no known competing financial interests or personal relationships that could have appeared to influence the work reported in this paper.

☐The authors declare the following financial interests/personal relationships which may be considered as potential competing interests:

Oxidation kinetic of soot generated from ammonia-acetylene laminar diffusion flame

Shuainan Yang[a], Chenyang Fan[a*], Zheng Fu[a,b], Ye Liu[c**], Huiyong Du[a], Bin Xu[a], Yidu Tong[a], Mingliang Wei[b]

[a] *Henan Provincial International Joint Laboratory of Energy Conservation and Pollutant Control of Energy Power Equipment, College of Vehicle and Traffic Engineering, Henan University of Science and Technology, Luoyang 471003, China*
[b] *State Key Laboratory of Intelligent Agricultural Power Equipment, Luoyang 471003, China*
[c] *Institute for Transport Studies, University of Leeds, Leeds LS2 9JT, UK*

Abstract
Co-combustion of ammonia with hydrocarbon fuels and its effect on soot emission characteristics have garnered interest. In this study, the oxidation kinetics of soot generated in a laminar co-flow acetylene diffusion flame were investigated under 30 –800 ℃ temperature-programmed oxidation and isothermal oxidation at 500℃, 600℃, and 700℃ using thermogravimetric analysis (TGA). The evolution of functional groups on soot surfaces and gaseous products were monitored by Fourier transform infrared spectroscopy (FT-IR) and thermogravimetric analysis coupled with infrared spectroscopy (TG-IR), respectively. Results indicate that the activation energy for soot oxidation increases with higher NH_3 substitution ratios (X_{NH_3}) and elevated temperatures. Isothermal oxidation tests also show that the oxidation rate constant increases with increasing X_{NH_3}. FTIR results show that increasing X_{NH_3} reduces aliphatic C–H groups and increases oxygenated groups on soot surfaces. The detected C–N bonds are attributed to dehydrogenation of aliphatic carbon atoms on polycyclic aromatic hydrocarbons (PAHs) surfaces. TG-IR analysis revealed the C–N bonds in urethanes on soot surfaces may release as the gaseous C–N species during low-temperature (500 ℃) oxidation of soot particles. Nevertheless, the higher-temperature facilitated the cleavage of C–N bonds, and then the generated NH_2 radicals react with oxygen radicals, leading to the formation of HNO on the soot surface.

Keywords: Ammonia; Soot; Functional groups; Oxidation; Reaction kinetics

*Corresponding author. E-mail address: fanchenyang@haust.edu.cn (C. Fan).

Novelty and significance statement

This work presents the first monitoring of the evolution of nitrogenated functional groups and gas products on the surface of soot with the progression of oxidation, sampled from C_2H_2/NH_3 flames. These results fill gaps in the understanding of the evolution of nitrogenated functional groups during soot oxidation and provide insights into nitrogen chemistry during this process, which is significant for reducing nitrogenated pollutant emissions.

1. Introduction

Ammonia (NH_3) is crucial for decarbonization initiatives, as its combustion does not release CO_2 [1, 2]. Nonetheless, the use of NH_3 has its drawbacks: low combustion stability [3], high ignition temperature [4] and low burning velocity [5]. An attractive way to overcome those shortcomings is to co-burn NH_3 with hydrocarbon [6, 7]. In this regard, Han et al. [5] showed that the maximum burning velocity could be enhanced by 340% when NH_3 is co-burned with CH_4 at substitution ratio of 0.4. Additionally, studies have reported significantly decreased combustion temperatures and enhanced flame stability when hydrocarbon fuels were mixed with NH_3 [8, 9].

In addition to the aforementioned benefits, another advantage of NH_3 co-combustion with hydrocarbons is the suppression of soot formation [10, 11]. Numerous studies have indicated that incorporating NH_3 into hydrocarbons during combustion significantly reduces the propensity for soot formation, given an equivalent carbon input [12, 13]. Bennett et al. [12] found that a 1% increase in the NH_3 mixing ratio resulted in a 4 –6% decrease in soot volume fraction (SVF) within C_2H_4 flames. Nitrogenated hydrocarbon species might be responsible for SVF reduction. Chu et al. [11] also found the reduction in SVF and polycyclic aromatic hydrocarbons (PAHs) content with the increase of ammonia ratio for the ammonia-

hydrocarbon blended fuel, whether in laminar or turbulent flames. Montgomery et al. [14] and Liu et al. [15] pointed out that a large number of hydrocarbons were consumed by nitrogenated species to form cyanide (CN) species, which would also result in a lower loading on soot. Therefore, the co-combustion of NH_3 with hydrocarbons reduces soot emissions through the inhibition of soot formation.

Although the inhibition of soot formation can effectively reduce soot emissions, soot oxidation is also an important factor in this reduction [16]. Soot oxidation kinetics is one of the essential factors in the soot oxidation mechanism. Soot oxidation kinetic is determined by a complex interplay of factors such as temperature [17], oxidation degree [18], nanostructure [19] and surface chemistry [20]. A disordered nanostructure, coupled with elevated temperatures, is inferred to expedite the soot oxidation kinetics [19, 21]. Several studies in the literature indicate that the concentration of oxygenated functional groups will convolve with soot nanostructure [22]. A higher abundance of oxygenated groups leads to soot nanostructures with more exposed edge-site carbon atoms, which are more readily oxidized [23, 24]. Due to the increasing popularity of alternative fuels, several researchers have investigated the impacts of fuel formulation on soot characteristics. Song [25] found that soot from soybean-derived biodiesel —an intrinsically oxygen-rich fuel —is five times more reactive than soot from Fischer-Tropsch diesel fuel. The authors suggested that the abundance of surface oxygenated functionalities is a critical factor influencing the oxidation rate. Vander Wal and Tomasek [26] showed that the soot particles generated by benzene, ethanol and acetylene have different nano-structural order and oxidation rate.

Recently, the effect of NH_3 application on soot oxidation has also been extensively investigated by assessing soot properties [27]. Zhang et al. [28] discovered that the addition of NH_3 in an ethylene co-flow diffusion flame increases the oxygen content on the soot surface, thereby affecting the oxidation process of soot. In addition, several studies [29, 30] have shown that the addition of NH_3 results in the introduction of nitrogenated functional groups to the soot surface. Liu et al. [15] experimentally detected C–N compounds such as HCN, H_3C_2N, and H_3C_3N using Gas Chromatography–Mass Spectrometry (GC–MS) in the 25 vol% NH_3-mixed flame. To gain further insight into the influence of nitrogenated functional groups on the soot oxidation process, Zhang et al. [30] analyzed the oxidation process of soot sampled from NH_3/C_2H_4 diffusion flames, pointing out that NH_3 consumed a large amount of hydrogen free radicals through $NH_3 + H \rightarrow NH_2 + H_2$ and $NH_2 + H \rightarrow NH + H_2$, while forming C–N bonds on the soot surface. Meanwhile, the reaction rates for the formation of OH via $H + O_2 \rightarrow OH + O$ and $H_2 + O \rightarrow OH + H$ are reduced, thereby affecting the oxidation process of soot. Li et al. [31] performed a study on the oxidation kinetics parameters of soot in an NH_3/toluene diffusion flame. They found that under 450 –700 ℃ programmed temperature oxidation, the activation energy (E_a) for soot oxidation decreased from 175 to 141 kJ·mol^{-1} as the NH_3 substitution ratio increased from 0% to 20%. They speculated that this phenomenon was attributed to the addition of NH_3, which induced HCN bonding and C–N formation on the soot surface, thereby inhibiting soot surface growth and affecting the nanostructure and soot oxidation process. Thus far, only limited studies have been carried out to investigate the oxidation behavior of soot following NH_3 addition [28, 31]. However, the complex evolution of nitrogenated functional groups during the soot oxidation process and the underlying mechanisms of their impact on soot oxidation kinetics remain unclear.

Thus, this study endeavors to investigate the effect of NH_3 addition on the oxidation kinetics of soot and the transformation of the surface functional groups, elucidating the pathways of functional groups' evolution during the oxidation process. The evolution of reaction kinetic parameters, gaseous oxidation products, and surface functional groups during the oxidation of soot under pure oxygen conditions was analyzed using Thermogravimetric analyzer (TGA), Fourier transform infrared spectrometry (FTIR) and TG-IR. The results assist in the design and optimization of particulate filters for NH_3 -blended diesel engines. Furthermore, the experimental results on the surface functional groups and oxidation reactivity of soot provide a valuable database for the development of more advanced soot models.

2. Experimental system and research methodology

2.1 Soot collection method and TGA analysis

In this study, particle samples were collected from a C_2H_2/air laminar co-flow diffusion flame on a Mckenna burner. The experimental schematic diagram of soot sampling is shown in Fig. 1. To investigate the effects of different NH_3 blending ratios on the oxidation reactivity of soot particles, soot samples were prepared through the combustion of a mixture of NH_3 and C_2H_2 fuel under controlled conditions. The detailed flow rate conditions are listed in Table 1. The substitution ratio of NH_3 in the fuel, X_{NH_3}, is defined as the mass fraction of NH_3 in the total fuel flow. For convenience, the fuel at X_{NH_3} of 0, 0.2, 0.4, and 0.6 is marked as N_{00}, N_{20}, N_{40}, and N_{60}, respectively. The X_{NH_3} was limited to 0.6 to prevent significant flame deformation and oscillation, ensuring that samples could be collected under stable and representative conditions. All gas flows were regulated by mass flow controllers (AB-11, AiroBoost) with an accuracy of 1% of the full scale.

The quartz plate was positioned near the tip of the stabilized flame to collect soot particles [31, 32], thereby minimizing disturbance to the flame structure. To minimize the chance of soot oxidation during

collection in any case, samples should not be taken for more than 5 minutes. The sampling methods used in the present work are based on our previous works by Jin et al [33]. Then, the quartz plate with deposited soot particles was washed with AR anhydrous ethanol (99.7%, Tianjin Beichen Fangzheng Reagent Factory), and anhydrous ethanol solution with dissolved soot particles can be obtained. The solution was centrifuged and dried for subsequent characterization.

In this study, a thermogravimetric analyzer (TGA2, Mettler-Toledo, Switzerland) was employed to evaluate the oxidation reactivity of soot samples during the temperature-programmed (TPO) and isothermal oxidation processes. Prior to the TPO test, the particle samples were thermally treated from room temperature to 400 ℃ with the heating rate of 15 ℃/min, and then were preserved at 400 ℃ for 30 min. Subsequently, the samples were cooled down to 30 ℃. After that, O_2 was introduced into the system at a flow rate of 50 mL/min to initiate the oxidation test. The whole TPO test was conducted from 30 ℃ to 800 ℃ with the heating rate of 5 ℃/min. The thermos-gravimetric (TG) curve, representing the mass loss during the oxidation process, and the differential thermogravimetric curve (DTG) were obtained according to the TPO test.

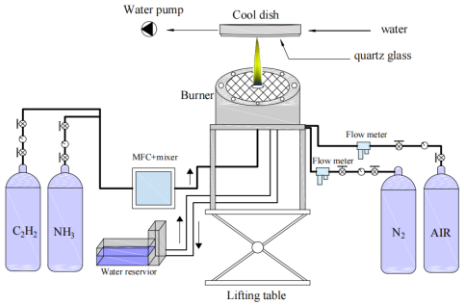

Fig. 1 Sampling device diagram

Table 1
Flow rate conditions for the present laminar diffusion flame.

case	C_2H_2 flow rate/(mL·min^{-1})	NH_3 flow rate/(mL·min^{-1})	N_2 flow rate/(mL·min^{-1})	Air flow rate/(L·min^{-1})	X_{NH_3}/%
N_{00}	200	0	300	20	0
N_{20}	200	100	200	20	20
N_{40}	200	200	100	20	40
N_{60}	200	300	0	20	60

Furthermore, isothermal tests were conducted at 500, 600, and 700 ℃ to investigate the oxidation kinetics, with the selected temperatures corresponding to typical conditions during engine diesel particulate filter (DPF) regeneration [34, 35]. Although the regeneration temperature of DPFs may fall below 500 ℃ in some cases, as pointed out by Ovaska [36], our preliminary isothermal results indicated that soot oxidation at such temperatures was moderate and exhibited a mass-loss profile similar to that observed at 500 ℃. Prior to the isothermal test, the procedure for SOF removal was also performed using the above-mentioned method. The soot oxidation degree (η) is the ratio of the mass reduced by the oxidation to the initial mass of the soot sample. During the isothermal oxidation, soot samples at various η were obtained by the following method: upon reaching the desired degree of mass loss (corresponding to the η), the heating was turned off and the oxidizing atmosphere was immediately switched to a pure nitrogen-inert atmosphere. Then the reaction chamber immediately cooled down to the room temperature with the rate of 50 ℃/min. The residual soot sample was taken out and sealed in a drying tank for further chemical analysis.

2.2 Chemical analysis techniques for soot samples

To monitor the type and concentration of functional groups within the soot samples, the soot samples were analyzed by a Fourier Transfer Inferred spectrometer (INVENIO-S, Bruker) that ran under a spectral range of 400 –4000 cm^{-1} with a resolution of 4 cm^{-1}. After the measurement under the set test conditions, the baseline of FT-IR spectrum was corrected and smoothed by OPUS software (Bruker). Each test was repeated more than three times to evaluate reproducibility. The results derived from these FT-IR spectra were averaged, with error bars representing the upper and lower deviations from multiple repeated experiments. The uncertainty of FT-IR results is less than 5 %.

2.3 TG-IR analysis

The soot sample TG-IR analyses were conducted using the FTIR spectrometer combined with the TGA. The gas products during the isothermal oxidation on TGA tests were introduced into the gas cell (A131-0100/TQ, Bruker) of FTIR through the customized tunnel. The customized tunnel was preserved at 220 ±5 ℃ to avoid gas condensation. The applied wavelength range of the FTIR spectra was from 4000 cm^{-1} to 400 cm^{-1} with a resolution of 4 cm^{-1}.

3. Results and discussion

3.1 Oxidation behavior of soot samples

Fig. 2 shows the TG curves for soot samples

generated under different NH_3 substituted ratios. To eliminate the influence of sample mass variations, the soot mass is normalized relative to the initial mass and presented as a percentage (%). The typical oxidation temperatures, representing of the oxidation reactivity of soot samples were derived from the TG curves according to the method suggesting in Li et al [31, 37]. Herein, the temperatures for maximum mass loss rate, the initial oxidation and burnout are respectively termed as T_{max}, T_i and T_e. The increasing substituted ratio of NH_3 resulted in a general decrease in T_{max}, T_i and T_e, as summarized in Table 2. Increasing the X_{NH_3} concentration from 0% to 20% results in a pronounced increase in the peak oxidation rate, from 12.9×10^{-3} to 14.6×10^{-3} mg/s. Further increasing the X_{NH_3} from 20% to 60% results in only a marginal enhancement of the peak oxidation rate, from 14.5×10^{-3} to 14.9×10^{-3} mg/s.

The oxidation kinetic parameters are further derived from TG curves using the Arrhenius-type equation [38, 39]:

$$-\frac{dm}{dt} = A\exp\left(\frac{-E_a}{RT}\right) m_c^{\ n} p_{o_2}^{\ r} \qquad \text{(Eq. 1)}$$

where m is the soot mass, m_c is the initial soot mass, t is the time, A is the pre-exponential factor (or frequency factor), E_a is the activation energy of the reaction, p_{O_2} is the partial pressure of oxygen, and n and r are the reaction orders of soot and oxygen, respectively. There is no consensus about the value of the reaction orders, but values close to unity (thus deriving in a first-order rate law) are hypothesized and/or found in the previous literature [23, 40, 41]. Since soot oxidation can be reasonably approximated as a unimolecular reaction under the present conditions, the reaction is assumed to follow first-order kinetics. From the equation, E_a and A can be estimated from the slope and intercept of the plot $\ln(-d(m/m_c)/dt)$ against $1/T$. Here, m/m_c represents the normalized soot mass, which can also be expressed in terms of the conversion degree α (i.e., $\alpha = 1 - m/m_c$).

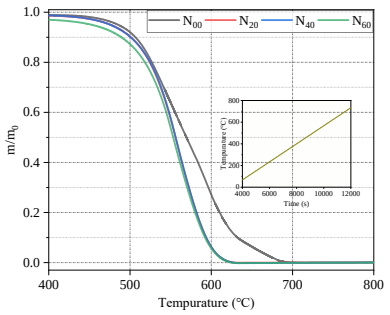

Fig. 2 Schematic diagram of the characteristic oxidation temperatures of soot with different X_{NH_3}.

As shown in Table 2, the E_a for soot samples obtained under different X_{NH_3} ranges from 114 to 145 kJ·mol^{-1}, with a remarked reduction as the X_{NH_3} increases. The E_a decreases significantly from 142.5 to 124.9 kJ·mol^{-1} as the X_{NH_3} increases from 0% to 20%. Increasing the X_{NH_3} from 20% to 40% resulted in a marginal decrease in E_a from 124.9 to 122.5 kJ·mol^{-1}, but the variation in E_a is within experimental uncertainty. Notably, as the X_{NH_3} increases from 40% to 60%, the E_a decreases by 6.9%, from 122.6 to 114.1 kJ·mol^{-1}. In the previous studies, the E_a for soot particles sampled from the hydrocarbon diffusion flames on burners ranges from 120.0 to 200.0 kJ·mol^{-1} [17, 42]. Li et al. [43] reported that the E_a of soot in a propane co-flow diffusion flame was 128−156 kJ·mol^{-1}. Liu et al. [44] collected soot samples at five axial positions in an ethylene laminar co-flow diffusion flame and found that the E_a varied between 150.0 and 180.0 kJ·mol^{-1}. Moreover, Ying et al. [45] found that the E_a of soot from the tip region of the C_2H_4 diffusion flame ranged from 127 to 139 kJ·mol^{-1}. It is found that E_a of soot obtained in the present study is rational in despite of the differences in X_{NH_3}. Similar results was also observed by Li et al. [31] who found a significant decrease in E_a from 175.0 to 141.0 kJ·mol^{-1} as the X_{NH_3} increased from 0% to 20% in a *n*-heptane diffusion flame.

Table 2
Oxidation kinetic parameters of soot from different X_{NH_3}.

condition	T_i/°C	T_{max}/°C	T_e/°C	Peak oxidation rate/mg·s^{-1}	E_a/kJ·mol^{-1}	R^2
N_{00}	520	594	620	12.9×10^{-3}	142.5	0.96
N_{20}	507	559	591	14.6×10^{-3}	124.9	0.95
N_{40}	506	557	576	14.7×10^{-3}	122.5	0.99
N_{60}	497	553	575	14.9×10^{-3}	114.1	0.97

Isothermal TG tests at 500 °C, 600 °C, and 700 °C were further conducted to scrutinize the oxidation kinetics. Fig. 3 shows the TG curves of soot particles with varying X_{NH_3} under pure oxygen condition at 500 °C, 600 °C, and 700 °C, respectively. The reaction rate constant k_c is calculated from the TG curves for soot samples according to Eq. 2.

$$-\frac{dm}{dt} = k_c m^n p_{O_2}^{\ r} \qquad \text{(Eq. 2)}$$

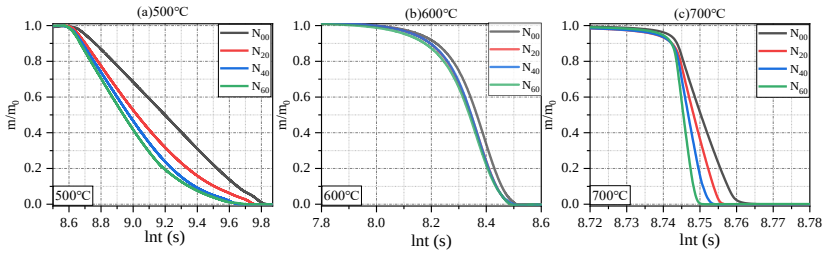

Fig. 3 Normalized mass loss curves of soot loss with different X_{NH_3}: (a) 500 ℃; (b) 600 ℃; (c) 700 ℃.

Fig. 4 shows k_c for soot at various oxidation degrees. At 500 °C, a substantially slower k_c is found and is two orders of magnitude lower than that for both 600 °C and 700 °C samples. The k_c at 600 °C is marginally lower than at 700 °C, by up to 41.5%. Under isothermal conditions, a monotonic decrease in k_c was observed with increasing X_{NH_3}, while at fixed X_{NH_3} values, k_c rises then falls with advancing soot oxidation degree. Similar oxidation behavior was observed by Jaramillo et al. [46] in representative soot samples of custom-synthesized onion-like carbon (OLC) using thermogravimetric analysis, with k_c values of ~10^{-7} (at 575 °C) increasing to ~10^{-5}(at 600 −700 °C)

The results demonstrate that NH_3 addition to acetylene flame reduces E_a of soot and enhances the k_c relative to that for pure acetylene fuel combustion. It is also found that a progressive reduction in k_c with increasing the degree of soot oxidation. These phenomena primarily arise from the following aspects.

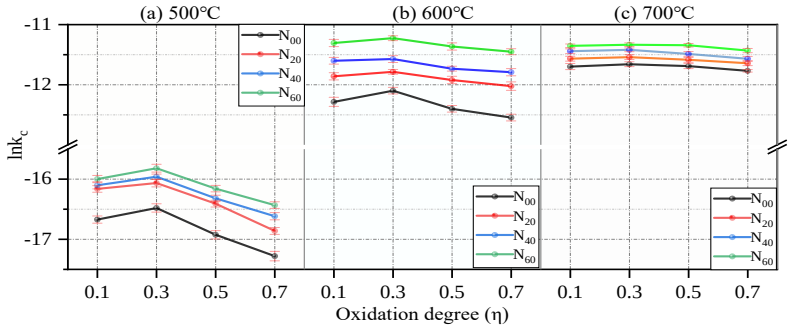

Fig. 4 The variation curve of k_c of soot with different X_{NH_3}: (a) 500 ℃; (b) 600 ℃; (c) 700 ℃

The variation in soot oxidative kinetic parameters may be responsible from the interaction of NH_3 with carbon atoms within the C_2H_2 during soot formation. This assertion can be supported by [13], where the decomposition of NH_3 in a NH_3/C_2H_4 flame was found to produce radicals which react with lighter hydrocarbons such as methyl (CH_3) radicals to form hydrogen cyanide (HCN). There was an obvious competitive mechanism between the addition reaction of HCN and C_2H_2, thereby suppressing soot nucleation and surface growth toward larger molecular structures, consequently inhibiting soot maturation [47, 48]. A similar inhibiting effect of NH_3 addition on soot formation was also observed by Zhang et al. [49]. They found that in NH_3-substituted ethylene laminar diffusion flames, NH_3 consumed a large amount of hydrogen radicals, leading to a notable reduction in the rate of the hydrogen-abstraction-acetylene-addition (HACA) reactions, ultimately inhibiting the nucleation and surface growth processes of soot. These similar phenomena was also observed in the studies of Bennett et al. [12], Ren et al. [50] , Yang et al. [51] and Cheng et al. [52]. The lessened growth and maturation of soot particles by NH_3 are prone to result in higher reactivity. The effects of NH_3 on the combustion natures, such as thermal, chemical, and dilution effects were also emphasized in the study of Yan et al. [53] to explain the activation of soot particles. Compared to hydrocarbon fuels, NH_3 addition reduces the lower heating value and varies the overall thermal and transport properties of the reactants, thus reducing the flame temperature field [54]. Meanwhile, NH_3 participates in the combustion reactions, generating new products that, in turn, regulate the reaction mechanisms. In addition, NH_3 participates in chemical reactions that produce HCN and nitrated polycyclic aromatic hydrocarbons (N-PAHs), thereby suppressing both soot formation and maturation. Ren et al. [50] observed that in C_2H_4-NH_3 flames, the nitrogen-hydrocarbon interactions promoted a new reaction pathway of NH_3 to produce hydrocarbon amines (CH_2CHNH_2, CH_3NH_2, CH_2NH, HCN, etc.). It blocked the carbon atoms in hydrocarbon radicals

(C_2H_2, C_2H_5, CH_3, etc.) originated from decomposition and oxidation of C_2H_4, thus affecting the subsequent PAH formation and soot growth. The dilution effect refers to the fact that NH_3 addition can affect the reaction process by reducing relative concentration of carbon-based fuels in the reactants. Zaher et al. [13] pointed out that the addition of NH_3 can inhibit nucleation and surface growth of soot primarily through thermal and chemical effects, rather than the dilution effect. This inhibition enhanced the soot oxidative reactivity by suppressing further soot maturation. The similar phenomena was also observed in the studies of Zhou et al. [55], Zhang et al. [49] and Wang et al. [56]. Previous studies [43, 57] found the soot deactivation as the oxidation proceeds. Liu [43] et al. observed that in a propane laminar co-flow diffusion flame, the E_a of mature soot collected at the flame tip exhibited a monotonic increase from 160 to 185 kJ·mol^{-1} as the oxidation degree increased from 0.3 to 0.9. In contrast, for the early-stage soot sampled from the flame of intermediate region, the E_a was approximately 135 kJ·mol^{-1} at the 30% conversion, decreased to a minimum of ~128 kJ·mol^{-1} at the 60% conversion, and subsequently increased to ~155 kJ·mol^{-1} at the 90% conversion. The oxidation-induced graphitization was employed to explain the deactivation of soot particles. As observed by Wang et al. [18], the structural ordering of soot in a propane co-flow diffusion flame increases monotonically with the soot oxidation degree.

The evolution of the gas phase products along the oxidation process can provide valuable insights into the oxidation kinetics involved in overall process. In this case, TG-IR and FT-IR techniques were employed in this work to detect the volatile products and functional groups on the solid soot surfaces evolved during soot oxidation.

3.2 TG-IR analysis of soot oxidation products

The TG-IR is used to analyze the evolution of gas-phase products during the oxidation reactions. To eliminate the influence of sample amount on peak area, the FT-IR spectrum obtained for each case are normalized relative to the peak area at ~1510 cm^{-1} (stretching of C=C). The typical band at ~1510 cm^{-1} is assigned to the asymmetric stretching vibration of aromatic C=C bonds during the pyrolysis and oxidation reactions, as revealed by Vikranth et al. [58], Liu et al. [59] and Yang et al. [60]. The peak area ratio (termed as A_x/A_{1510}, where x represents the peak position of the corresponding species) of specific functional groups to the aromatic C=C group can represent the concentration of functional groups [33, 61]. Figs. 5 −7 present the FT-IR spectra of the gas-phase products during soot oxidation at 500 °C, 600 °C, and 700 °C, respectively. It is evident that all FT-IR spectra exhibit a similar adsorption pattern with nearly identical peak positions, indicating a comparable composition of functional groups present during the oxidation process. However, variations in the area of the individual peaks are also observed in the FT-IR spectra, indicating differences in the distribution and amount of functional groups. Therefore, a quantitative analysis was conducted by deconvolution of the FT-IR spectra using Gaussian functions.

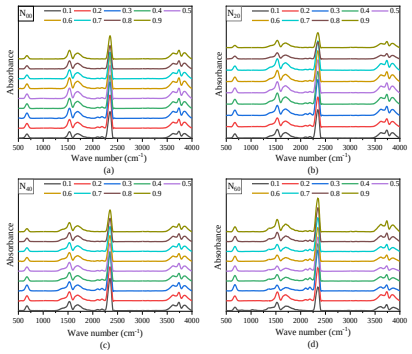

Fig. 5 Absorption spectra at 500 °C with different η: (a) N_{00}; (b) N_{20}; (c) N_{40}; (d) N_{60}.

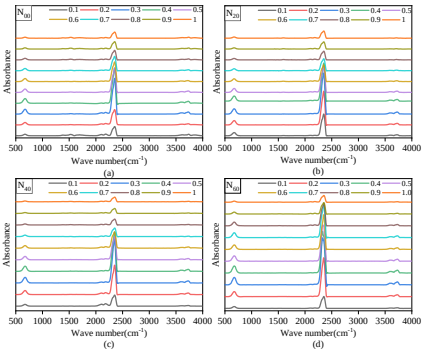

Fig. 6 Absorption spectra at 600 °C with different η: (a) N_{00}; (b) N_{20}; (c) N_{40}; (d) N_{60}.

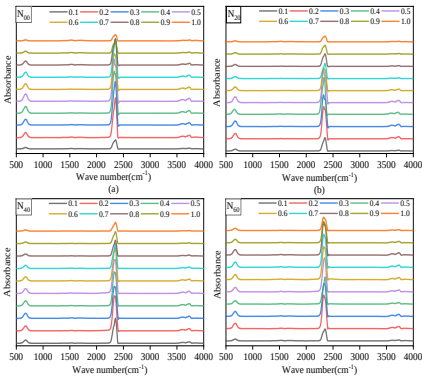

Fig. 7 Absorption spectra at 700 °C with different η: (a) N_{00}; (b) N_{20}; (c) N_{40}; (d) N_{60}.

As shown in Figs. 5 –7, less absorption peaks for gaseous oxidation products are detected at 600 °C and

700 °C in comparison with that for 500 °C. It may arise from the substantial enhancement of soot oxidation and CO_2 generation at elevated temperatures, suppressing formation of other products. In addition, it is evident that CO_2 is the predominant gaseous oxidation product in the soot oxidation process. This is characterized by two distinct FTIR absorbance bands at 670 cm^{-1} (C=O symmetric stretching) and 2360 cm^{-1} (C=O asymmetric stretching) [62, 63], respectively. The absorption band near 2179 cm^{-1} is attributed to the C–O stretching vibration of CO [64, 65]. The absorption bands observed at 3400 –4000 cm^{-1} are attributed to the stretching vibration of –OH groups, which likely originate from carboxylic acids and phenols produced during soot oxidation [66, 67]. However, these peaks are easily interfered by the –OH within water molecules in lab atmosphere [33]. Therefore, this spectral range was not further analyzed. The peak at 1310 –1370 cm^{-1} is attributed to nitrogenated functional group stretching vibrations [68-70]. Zhao et al. [69] identified characteristic FT-IR absorption bands at ~1537 cm^{-1} (N–H bending vibration) and ~1310 cm^{-1} (C–N stretching vibration) during the thermal degradation of polyurethane foam in nitrogen and air atmospheres. These observations can be attributed to the presence of urethane functional groups. Similar results were also observed by Lan et al. [70], who found that the thermal decomposition of 3-nitro-1,2,4-triazol-5-one (NTO), as analyzed using FT-IR spectroscopy, exhibited characteristic absorption bands corresponding to the NO_2 symmetric stretching vibration at 1380 –1360 cm^{-1} and the C≡N stretching vibration at 1680 –1370 cm^{-1}. The phenomena indicate the presence of characteristic absorption bands associated with nitrogenated functional groups in the spectral regions around 1310 and 1380 cm^{-1}. According to the previous studies, the band at 1300 –1370 cm^{-1} originates from either the escape of C–N bonds in urethane [69] or the NO_2 [70]. In addition, as proposed by Ren et al. [71], who observed using Microscopic imaging infrared spectrometer (MIR), the soot sampled from a C_2H_4/NH_3 laminar diffusion flame exhibited a notable characteristic peak at 2221 cm^{-1}, representing C≡N bond tensile vibration of aromatic hydrocarbons. The band for C=O (coming from ketones, esters, anhydrides and lactones) is observed in the range of 1650 –1860 cm^{-1} [72]. The peak centered at ~1510 cm^{-1} corresponds to the C=C (1510 cm^{-1}) stretching vibration in the range of 1600 –1420 cm^{-1}.

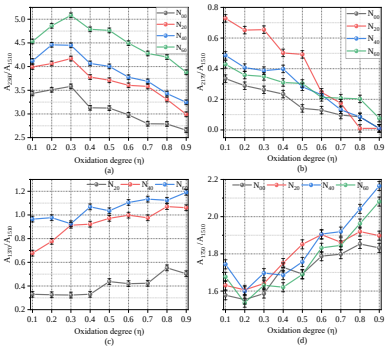

Fig. 8 Concentrations of gas-phase products from soot samples with varying η at 500 °C: (a) CO_2; (b) CO; (c) Nitrogenated functional group; and (d) C=O.

The evolution of A_{2360}/A_{1510} and A_{2179}/A_{1510} (CO_2 and CO products, respectively) along the oxidation process at 500°C is presented in Figs. 8 (a) and (b). The A_{2360}/A_{1510} shows a significant increase as the oxidation degree increases from 0.1 to 0.3, while exhibiting a progressive reduction upon further oxidation degree from 0.4 to 0.9. The evolution of A_{2360}/A_{1510} aligns with that for k_c. CO_2 is the predominant gaseous oxidation product in the soot oxidation process. Therefore, CO_2 production effectively reflects both the oxidation rate and oxidative kinetics [66, 73]. The similar phenomena was also observed in the studies of Liu et al [43] and Wang et al [18]. Liu et al. found that in propane co-flow diffusion flames, with the increasing soot oxidation degree, the soot oxidation reactivity first increases and then decreases. Unlike A_{2360}/A_{1510}, A_{2179}/A_{1510} decreases linearly with increasing oxidation degree. At an oxidation degree of 0.9, A_{2179}/A_{1510} is nearly negligible. In addition, it is observed that A_{2179}/A_{1510} does not show significant systematic variation with increasing X_{NH_3}. Conversely, increase in X_{NH_3} leads to the increase in A_{2179}/A_{1510} at the same oxidation degree. The increasing oxidation reactivity of soot particle results from NH_3 addition [28, 31], may be the plausible factor for the increase in A_{2179}/A_{1510} In a NH_3/C_2H_4 co-flow diffusion flame, Zhang et al. [28] indicates that the addition of NH_3 can enhance the content of oxygenated functional groups in soot particles. The oxygenated compounds (methoxy, –COOH, C=O, ether, phenolic –OH, etc.) on particle surfaces undergo fragmentation and oxidation of carbon atoms, primarily releasing CO_2, as observed by Wei et al. in their study.

Fig. 8 (c) shows the evolution of A_{1370}/A_{1510} during soot oxidation. A_{1370}/A_{1510} shows a gradual increase as soot oxidation degree progresses from 0.1 to 0.9. In addition, with the increasing X_{NH_3}, A_{1370}/A_{1510} increased, whereas no significant band at ~1370 cm^{-1} was detected for X_{NH_3}= 0, indicating that the band at ~1370 cm^{-1} originates only from the NH_3 combustion and its effect on soot formation. This assertion can be supported by Shao et al. [74] who found that in a

NH_3/C_2H_4 laminar premixed flame, NH_3 addition enhances carbon-nitrogen interactions and the formation of nitrogen oxides and nitrogenated species including HCN and N-PAHs. Fig. 8 (d) shows that A_{1750}/A_{1510} increases as the oxidation process progressed at 500 °C. This phenomenon likely originates from the desorption of lipids, alcohols, phenols, and ethers from soot surfaces, coupled with carbon-oxygen interactions during the oxidation process.

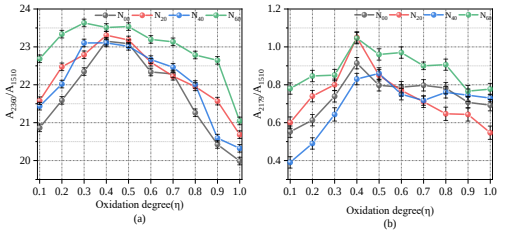

Fig. 9 Concentrations of gas-phase products from soot samples with varying η at 600 °C: (a) CO_2 absorption band area; (b) CO absorption band area.

Relative to that for 500 °C, soot oxidation at 600 °C (see Fig. 9) and 700 °C (see Fig. 10) result in substantial increase in A_{2360}/A_{1510}. The improved k_c at elevated temperatures may be responsible for the higher CO_2 emission, as afore-discussed [17]. In addition, at 600 °C, similar to the behavior at 500 °C, A_{2360}/A_{1510} increases as η increases from 0.1 to 0.4, then gradually decreases as oxidation progresses from 0.4 to 1.0, in agreement with the behavior of k_c as η increases. However, unsimilar to that for 500 °C and 600 °C, A_{2360}/A_{1510} exhibits marginal variations with the oxidation process at 700 °C. The data also observed that k_c remains nearly constant as the degree of oxidation increases at 700 °C. The experimental observations indicate that at elevated temperatures, temperature is likely the primary factor influencing soot oxidation rates, while the impact of intrinsic reactivity is diminished. In addition, it is observed that, unlike at 500 °C, A_{2179}/A_{1510} initially increases and then decreases during the soot oxidation process at 600 °C, whereas remains virtually undetectable during the oxidation process at 700 °C. This phenomenon likely arises from the promoted oxidation of CO to CO_2 at elevated temperatures during the process of soot oxidation.

Consistent with the behavior observed at 500 °C, A_{2360}/A_{1510} increases with increasing X_{NH_3} at 600 °C and 700 °C, indicating that the NH_3 addition enhances soot oxidation rate and accelerates the oxidation process [31, 50, 74]. Notably, at 600 °C and 700 °C, the A_{1370}/A_{1510} fall below detectable limits as the X_{NH_3} increases.

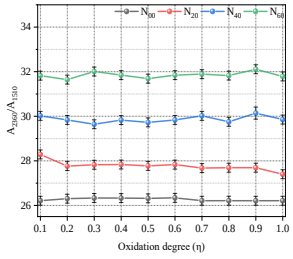

Fig. 10 Concentrations of CO_2 from soot samples with varying degrees of oxidation at 700 °C.

3.3 *Soot bulk chemistry*

FT-IR spectroscopy was employed to identify and quantify the functional groups on the soot surface. In this study, the FT-IR spectra for each sample are normalized against the band intensity at ~1620 cm^{-1} (assigned to the aromatic C=C stretching vibration) to eliminate sample size effects on band intensities [75, 76]. From Figs. 11 −13, it is evident that the soot samples exhibit infrared absorbance at the same peak positions, but distinctly different absorbance intensity for different X_{NH_3} and η, indicating the difference in the composition of soot functional groups.

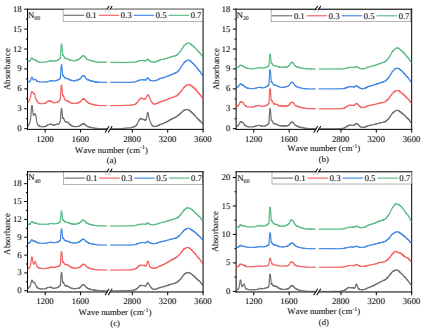

Fig. 11 Absorption spectra of soot samples at varying η at 500 °C: (a) N_{00}; (b) N_{20}; (c) N_{40}; (d) N_{60}.

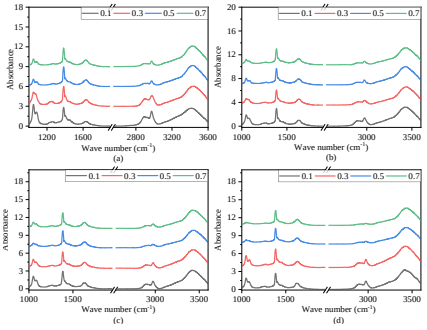

Fig. 12 Absorption spectra of soot samples at varying η at 600 °C: (a) N_{00}; (b) N_{20}; (c) N_{40}; (d) N_{60}.

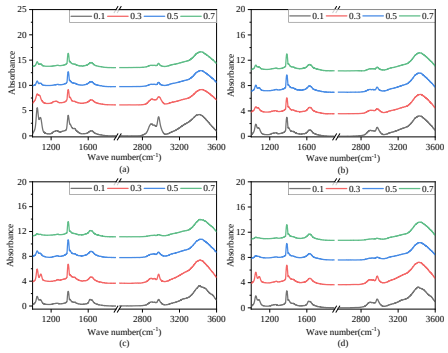

Fig. 13 Absorption spectra of soot samples at varying η at 700 °C: (a) N_{00}; (b) N_{20}; (c) N_{40}; (d) N_{60}.

Figs. 11 −13 present the FT-IR spectra of the soot surface during soot oxidation at 500 °C, 600 °C, and 700 °C, respectively. The most intense absorption occurs at 3300 –3650 cm^{-1}, which corresponds to the stretching vibration of –OH groups [75, 76], likely originating from carboxyls and phenols produced during soot oxidation [67, 68]. However, these peaks are easily interfered by the –OH within water molecules in lab atmosphere [68], so it is difficult to determine whether it arises from those bound by soot surfaces. Consequently, the peaks in this range are not analyzed in this study. The peaks at 2975, 2925 and 2860 cm^{-1} correspond to the aliphatic C–H functional groups [33, 77]. The areas of the peaks at 2950, 2925, and 2860 cm^{-1} are integrated to assess the total concentration of the aliphatic groups in this work. The peaks corresponding to C=O groups (from ketones, esters, anhydrides, and lactones) are approximately located at 1700 cm^{-1}, as stated in reference [68] within the range of 1650 –1860 cm^{-1}. The peaks centered at ~1620 cm^{-1} corresponds to the vibration peak of aromatic C=C [67, 78]. The peak area ratio $A^{(s)}{}_x/A^{(s)}{}_{1620}$ (x represents the peak position of specific functional groups on the solid surfaces of soot samples) corresponds to the concentration of functional groups [79]. The peaks centered at ~1250 cm^{-1} corresponds to the stretching of the C–O bands of phenolic, anhydride, ester, and ether-like groups [18].

Owing to the presence of N atoms in NH_3, the C–N groups and other nitrogenated species are specially scrutinized to shed light on the effect of NH_3 on soot properties. The peaks centered at ~1350 cm^{-1} are detected and probably arising from the stretching vibrations of C–N groups in urethane [69]. From the pyrolysis of flexible polyurethane foam (FPUF), Zhao et al. [69] stated the absorption at 1310 cm^{-1} arise from the C–N stretching vibrations in urethane. However, Tapia et al. [80] observed a distinct absorption peak at 1354 cm^{-1} for diesel soot when exposed to NO_2, as determined by Diffuse Reflectance Infrared Fourier Transform Spectroscopy (DRIFTS) analysis. They postulated that nitro-compounds are generated during the oxidation of soot oxidation via electrophilic substitution in the presence of NO_2, resulting in the formation of N-PAHs. Additionally, in their study on the interaction between diesel soot and NO_2, Azambre et al. [81] detected the absorption band near 1370 –1300 cm^{-1} using DRIFTS. They hypothesized that this phenomenon might be attributed to the chemisorption of NO_2 at the surface sites of diesel soot particles, thereby inducing the formation of nitrogenated (RNO_X) adsorbed intermediates on the soot surface. Nevertheless, the observations mentioned above only confirm the presence of nitrogenated polycyclic aromatic hydrocarbons, however, they do not elucidate the specific bonding configurations of nitrogen atoms within the aromatic structures. In the study on the surface functional groups of biomass fuel particles, Popovicheva et al. [82] identified prominent bands of aromatic nitro-compounds (NO_2 stretching vibrations) in the range of 1320 –1355 cm^{-1} via FTIR analysis. They supposed that the formation of this substance could be linked to the increased emission of nitrogen oxides (NO_X) and nitro-PAH from biomass fuel engines [83, 84]. Incorporating both the existing literature and the present experimental data, the observed variations in the 1300 –1370 cm^{-1} spectral region are tentatively attributed to the substitution of nitrogenated functional groups following the dehydrogenation of aliphatic carbon atoms bonded to PAH surfaces.

Fig. 14 presents the evolution of surface groups during oxidation at 500 °C. $A^{(s)}{}_{2860}/A^{(s)}{}_{1620}$ shows a progressive decrease with the increasing η, indicating the consumption of aliphatic C–H bonds via dehydrogenation and carbonization reactions occurring on the soot surface during the oxidation process [18, 67]. Opposite to the increase of A_{2360}/A_{1510} (from CO_2) for the afore-discussed gas products, the $A^{(s)}{}_{1700}/A^{(s)}{}_{1620}$ and $A^{(s)}{}_{1250}/A^{(s)}{}_{1620}$ decrease gradually during oxidation at 500 °C as the η increases from 0.1 to 0.3. This phenomenon is likely attributable to decarboxylation occurring on the soot surface, which releases C–O and C=O functional groups and results in the evolution of CO_2 [81, 85]. Nevertheless, as η increases from 0.3 to 0.5, $A^{(s)}{}_{1700}/A^{(s)}{}_{1620}$ and $A^{(s)}{}_{1250}/A^{(s)}{}_{1620}$ continue to decrease, accompanying with the reduction in A_{2360}/A_{1510} (from CO_2) for the gaseous product. Upon increasing η from 0.5 to 0.7, $A^{(s)}{}_{1700}/A^{(s)}{}_{1620}$ and $A^{(s)}{}_{1250}/A^{(s)}{}_{1620}$ increase, indicating the accumulation of oxygenated functional groups on the surface of carbon soot during this stage.

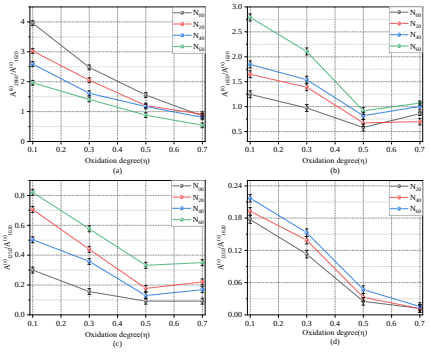

Fig. 14 Concentrations of (a) Aliphatic C–H, (b) C=O, (c) C–O in COOH and (d) C–N functional groups of soot samples with varying degrees of oxidation at 500 °C

Additionally, the addition of NH_3 could increase the C=O and C–O groups in soot particles, as evidenced by the increase in $A^{(s)}_{1700}/A^{(s)}_{1620}$ and $A^{(s)}_{1250}/A^{(s)}_{1620}$ with increasing X_{NH_3}. As supported by the results of E_a and k_c, the addition of NH_3 enhances the reactivity of soot oxidation, which probably stems from oxidation-induced ordering of soot, resulting in increases in the number of active sites on the surface of soot particles available for reaction with oxygenated radicals [28]. As the oxidation progresses, $A^{(s)}_{1350}/A^{(s)}_{1620}$ decreases monotonically, indicating that nitrogenated functional groups on the soot surface are progressively removed and released with the gas-phase during the oxidation process, as evidenced by the progressive increase in A_{1370}/A_{1510} in the gaseous oxidation products. Additionally, with increasing X_{NH_3}, $A^{(s)}_{1350}/A^{(s)}_{1620}$ gradually increases, indicating that the addition of NH_3 promotes an increase in nitrogenated functional groups on the soot surface. Similar effects of NH_3 addition on the soot surface composition was also found by Zaher et al. [86]: for a NH_3–C_2H_4 flame, the increase in NH_3 concentration leads to the formation of more carbon-nitrogen (C–N) bonds at the soot surface. Absorption bands at 1310 ~1370 cm^{-1} were also detected by Zhao et al. [69] and Tapia et al. [87] for the soot samples. For instance, Zhao et al. [69] assigned the band at 1310 cm^{-1} to the C–N stretching vibrations in urethane. Tapia et al. [87] pointed out that the absorption peak at 1354 cm^{-1} stemmed from the C–N groups in N-PAHs generated from the nitro compounds during the oxidation of soot by NO_2. By microscopic imaging infrared spectrometer (MIR), Ren et al. [71] found the stretching vibration of C–N bonds in aromatic compounds at 2221 cm^{-1} for the soot collected from a C_2H_4 –NH_3 co-flow laminar diffusion flame. They proposed that the N-PAHs were generated from the hydrogen substitution by hydrogen cyanide (HCN) and cyanide (CN) on the aromatic ring. For these cases, an assertion can be proposed that the peak at 1350 cm^{-1} may be attributed to the formation of aliphatic C–N bonds attached on PAH matrixes.

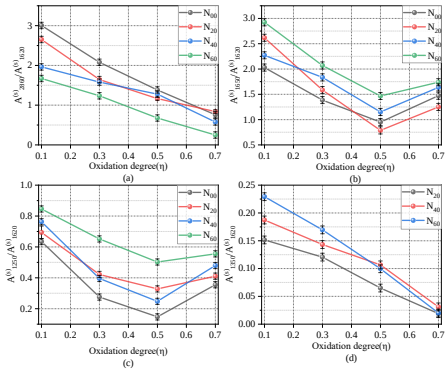

Fig. 15 Concentrations of (a) Aliphatic C–H, (b) C=O, (c) C–O in COOH and (d) C–N functional groups of soot samples with varying degrees of oxidation at 600 °C.

Figs. 15 and 16 show the evolution of surface functional groups on soot during oxidation at 600 °C and 700 °C, respectively. Consistent with the behavior observed at 500 °C, $A^{(s)}_{2860}/A^{(s)}_{1620}$ decreases with increasing η, indicating that the aliphatic C–H bonds on the soot surface are gradually consumed during the oxidation process. Simultaneously, some aliphatic C–H bonds may be transformed and released as volatile oxygenated functional groups, as evidenced by the increase in A_{1750}/A_{1510} with rising η. In addition, as η increases, $A^{(s)}_{1350}/A^{(s)}_{1620}$ gradually decreases, while the gas-phase product A_{1370}/A_{1510} correspondingly increases. As the oxidation progresses, the C–N bonds on the soot surface gradually escape into the gas phase. Nevertheless, although C–N bonds are detected on the solid soot surface when the temperature exceeds 600 °C, the fluctuations of C–N species in the gas-phase products become virtually negligible as the oxidation proceeds. Concurrently, aromatic N–O groups were detected on the soot particle surface near 1500 –1570 cm^{-1} [82]. A potential explanation is that, under elevated temperature conditions, the C–N bonds predominantly participate in reactions on the solid surface of soot. The higher temperature may facilitate the cleavage of C–N bonds within urethane molecules on the soot surface. Subsequently, the resulting NH_2 groups present on the soot surface may react with oxygen radicals, potentially leading to the formation of HNO on the soot surface. This reaction may potentially hinder the migration of C–N bonds from the soot surface to the gas phase. In summary, as the temperature increases, the significant increase in E_a and k_c indicates a heightened propensity for the oxidation of soot particles, as evidenced by the variation in gaseous products generated during the soot oxidation process. CO_2, as the primary product of soot oxidation, shows a significant increase in concentration as the oxidation temperature rises. This observation underscores that elevated temperatures significantly accelerate the conversion of C–H bonds on the soot surface to gaseous CO_2. The formation of CO_2, enhanced by the elevated temperature, may simultaneously hinder the generation of other gaseous products. Additionally, as X_{NH_3} increases, both the E_a and the k_c are elevated, suggesting that the addition of NH_3 enhances the soot oxidation.

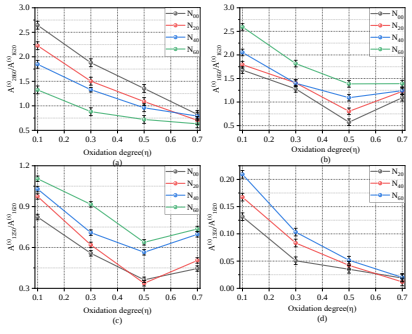

Fig. 16 Concentrations of (a) Aliphatic C–H, (b) C=O, (c)

C–O in COOH and (d) C–N functional groups of soot samples with varying degrees of oxidation at 700 ℃.

4. Conclusions

To investigate the effects of ammonia addition on soot oxidation kinetics in acetylene diffusion flames, soot samples were collected from flames at various NH_3 substitution ratios (X_{NH_3}). The soot samples were characterized by thermogravimetric analysis (TGA), Fourier transform infrared spectroscopy (FTIR), and thermogravimetric-infrared spectroscopy (TG-IR). The results from temperature programmed oxidation indicated that, as X_{NH_3} and oxidation temperature increase, the activation energy (E_a) for soot oxidation increase. Isothermal oxidation test proved that rate constant (k_c) for soot oxidation was elevated by the increase in X_{NH_3}. Additionally, k_c showed an initial increase and then decrease as the isothermal oxidation evolves. From the FTIR results, the concurrent reduction of aliphatic C–H groups and increase in oxygenated groups was found with increasing X_{NH_3}. The C–N bond was also detected on soot surfaces and was attributed to the dehydrogenation of aliphatic carbon atoms attached to the surface of polycyclic aromatic hydrocarbons (PAHs). The TG-IR analysis revealed the C–N bonds in urethanes on soot surfaces may adsorb and/or release as the gaseous C–N species during the low-temperature (500 ℃) oxidation of soot particles. Nevertheless, under high-temperature conditions of 600 ℃ and 700 ℃, nitrogenated species were not detected in the gaseous products, while N–O groups were detected on the soot solid surface at 1500 –1570 cm^{-1} in the adsorption spectra. It was speculated that the elevated oxidation temperature facilitated the cleavage of C–N bonds within urethane molecules on the soot surface, and then the generated NH_2 radicals may react with oxygen radicals, leading to the formation of HNO.

CRediT authorship contribution statement

Shuainan Yang: Conceptualization, Investigation, Data visualization, Writing-original draft. **Chenyang Fan**: Investigation, Methodology, Funding acquisition, Project administration, Writing-review & editing. **Zheng Fu**: Investigation, Resources, Data visualization. **Ye Liu**: Investigation, Data visualization. **Huiyong Du**: Methodology, Resources. **Bin Xu**: Methodology, Resources. **Yidu Tong**: Investigation, Data visualization, Validation. **Mingliang Wei**: Data Curation, Data visualization.

Declaration of competing interest

The authors declare that they have no known competing financial interests or personal relationships that could have appeared to influence the work reported in this paper.

Acknowledgments

This research is sponsored by National Natural Science Foundation of China (No. 52006054), and International scientific and technological cooperation project in Henan Province (No. 232102521019)

References

[1] L.W. Kang, W.G. Pan, J.K. Zhang, et al., A review on ammonia blends combustion for industrial applications, Fuel 332 (2023) 126150.
[2] P. Berwal, S. Kumar, B. Khandelwal, A comprehensive review on synthesis, chemical kinetics, and practical application of ammonia as future fuel for combustion, J. Energy Inst. 99 (2021) 273-98.
[3] J.W. Ku, S. Choi, H.K. Kim, et al., Extinction limits and structure of counterflow nonpremixed methane-ammonia/air flames, Energy 165 (2018) 314-25.
[4] C. Zamfirescu, I. Dincer, Ammonia as a green fuel and hydrogen source for vehicular applications, Fuel Process. Technol. 90 (2009) 729-37.
[5] P. Berwal, Shawnam, S. Kumar, Laminar burning velocity measurement of CH4/H2/NH3-air premixed flames at high mixture temperatures, Fuel 331 (2023) 125809.
[6] A.J. Reiter, S.C. Kong, Combustion and emissions characteristics of compression-ignition engine using dual ammonia-diesel fuel, Fuel 90 (2011) 87-97.
[7] K. Ryu, G.E. Zacharakis-Jutz, S.C. Kong, Effects of gaseous ammonia direct injection on performance characteristics of a spark-ignition engine, Appl. Energy 116 (2014) 206-15.
[8] E.C. Okafor, Y. Naito, S. Colson, et al., Experimental and numerical study of the laminar burning velocity of CH4–NH3–air premixed flames, Combust. Flame 187 (2018) 185-98.
[9] O. Kurata, N. Iki, T. Matsunuma, et al., Performances and emission characteristics of NH3–air and NH3CH4–air combustion gas-turbine power generations, Proc. Combust. Inst. 36 (2017) 3351-9.
[10] W.L. Dong, J.F. Yao, R. Hong, et al., Atomic insights into the mechanism of ammonia inhibiting soot formation during pyrolysis of new bio-oxygenated fuels, Renew. Energy 256 (2026) 124035.
[11] H.Q. Chu, S.J. Feng, R. Hong, et al., Effects of ammonia addition on soot formation in hydrocarbon fuels combustion: Challenges and prospects, Fuel 360 (2024) 130569.
[12] A.M. Bennett, P. Liu, Z. Li et al., Soot formation in laminar flames of ethylene/ammonia, Combust. Flame 220 (2020) 210-8.
[13] M.H. Zaher, C. Chu, M. Dadsetan, et al., Experimental and numerical investigation of soot growth and inception in an ammonia-ethylene flame, Proc. Combust. Inst. 39 (2023) 929-37.
[14] M.J. Montgomery, H. Kwon, J.A.H. Dreyer, et al., Effect of ammonia addition on suppressing soot formation in methane co-flow diffusion flames, Proc. Combust. Inst. 38 (2021) 2497-505.
[15] Y. Liu, X. Cheng, Y. Li, et al., Effects of ammonia addition on soot formation in ethylene laminar diffusion flames, Fuel 292 (2021) 120416.
[16] M. Athanasios, Feasibility of Introducing Particulate Filters on Gasoline Direct Injection Vehicles. A Cost Benefit Analysis, Report No. JRC66723, European

Commission Joint Research Center-Institute for Energy and Transport, Ispra, Italy, 2011.
[17] I.C. Jaramillo, C.K. Gaddam, R.L. Vander Wal, et al., Soot oxidation kinetics under pressurized conditions, Combust. Flame 161 (2014) 2951-65.
[18] X. Wang, J. Wei, Y. Zeng, et al., Diesel soot combustion in air-NO environment: Evolution of functional groups on soot surfaces, Sci. Total Environ. 918 (2024) 170579.
[19] L.X. Wang, F. Ren, X.G. Cheng, et al., Insight of soot nanostructure and oxidation behavior in ammonia/ethylene coaxial diffusion flame, Fuel 349 (2023)128629.
[20] C. Russo, A. Ciajolo, S. Cimino, et al., Reactivity of soot emitted from different hydrocarbon fuels: Effect of nanostructure on oxidation kinetics, Fuel Process. Technol. 236 (2022) 107401.
[21] Y. Liu, Y. Xu, K. Zhang, et al., Effects of ammonia addition on soot formation in ethylene laminar diffusion flames. Part 3. The morphology and nanostructure of soot particles, Fuel 332 (2023) 126082.
[22] R.L. Vander Wal, V.M. Bryg, M.D. Hays, XPS analysis of combustion aerosols for chemical composition, surface chemistry, and carbon chemical state, Anal. Chem. 83 (2011) 1924-30.
[23] J. Song, M. Alam, A.L. Boehman, Impact of alter-native fuels on soot properties and DPF regeneration, Combust. Sci. Technol. 179 (2007) 1991-2037.
[24] N. Serhan, A. Tsolakis, F.J. Martos, Effect of propylene glycol ether fuelling on the different physico-chemical properties of the emitted particulate matters: Implications of the soot reactivity, Fuel 219 (2018) 1-11.
[25] J. Song, Effect of fuel formulation on soot properties and regeneration of diesel particulate filters, Proceedings of the Diesel Engine Emissions Reduction Conference (2005), paper 20154401487632.
[26] R.L. Vander Wal, A.J. Tomasek, flame, Soot oxidation: dependence upon initial nanostructure, Combust. Flame 134 (2003) 1-9.
[27] W.L. Dong, R. Hong, Y.H. Yang, et al., Analysis of the nanostructure evolution of soot in nheptane/iso-octane with 2,5-dimethylfuran addition: A combined experimental study and ReaxFF MD simulations, Combust. Flame 270 (2024) 113751.
[28] F. Zhang, S.L. Li, Q.Q. Liu, et al., Effect of ammonia on the soot surface characteristics in ammonia/ethylene co-flow diffusion flames, Fuel 341 (2023) 127633.
[29] H. Zhou, L. Yan, Y.H. Yang, et al., Synergistic catalytic effect of Mo and Ni on the nitrogen-doped carbon nanotubes in an axisymmetric laminar co-flow ethylene/ammonia/air diffusion flame, Carbon 238 (2025) 120232.
[30] K. Zhang, Y. Xu, Y. Liu, et al., Effects of ammonia addition on soot formation in ethylene laminar diffusion flames. Part 2. Further insights into soot inception, growth and oxidation, Fuel 331 (2023) 125623.
[31] Q. Li, B. Tian, L. Xu, et al., Effects of ammonia addition on the soot nanostructure and oxidation reactivity in n-heptane/toluene diffusion flames, Fuel Process. Technol. 257 (2024) 108090.
[32] Y. Zhang, A.L. Boehman, Oxidation behavior of soot generated from the combustion of methyl 2-butenoate in a co-flow diffusion flame, Combust. Flame 160 (2013) 112-9.
[33] S. Jin, C. Fan, Z. Fu, et al., Adsorption and oxidation of NO and N2O on soot surfaces: Evolution of functional groups, Fuel 390 (2025) 134643.
[34] P. Tan, B. Cui, L. Duan, et al., Pressure drop model of DPF considering ash factor at different capture stages, Energy 283 (2023) 128439.
[35] Y.J. Chen, P.Q. Tan, L.S. Duan, et al., Temperature, particulate emission characteristics, and emission reduction performance for SCR coated on DPF under drop to idle regeneration, Energy 268 (2023) 126764.
[36] T. Ovaska, K. Spoof-Tuomi, S. Niemi, et al. Performance during a period of late diesel injection for DPF regeneration, proceedings of asme. ASME ICE Forward (2024) 113406.
[37] J.F. Luo, Y.M. Zhang, J. Wang, et al., Effect of acetone-butanol-ethanol addition to diesel on the soot reactivity, Fuel 226 (2018) 555-63.
[38] H.L. Friedman, Kinetics of thermal degradation of char-forming plastics from thermogravimetry. Application to a phenolic plastic, J. Polym. Sci., Part C: Polym. Symp. 6 (1964) 183-95.
[39] J. Rodríguez-Fernández, F. Oliva, R.A. Vázquez, Characterization of the Diesel Soot Oxidation Process through an Optimized Thermogravimetric Method, Energy Fuels 25 (2011) 2039-48.
[40] B. Dernaika, D. Uner, A simplified approach to determine the activation energies of uncatalyzed and catalyzed combustion of soot, Appl. Catal. B: Environ. 40 (2003) 219-29.
[41] G. Stratakis, A.M. Stamatelos, Thermogravimetric analysis of soot emitted by a modern diesel engine run on catalyst-doped fuel, Combust. Flame 132 (2003) 157-69.
[42] P. Ciambelli, P. Corbo, M. Gambino, et al., Catalytic combustion of carbon particulate, Catal. Today. 27 (1996) 99-106.
[43] P. Liu, S.Y. Li, Influence of maturity on the oxidation kinetics and nanostructure evolution of soot sampled from a propane coflow diffusion flame, Prog. React. Kinet. Mech. 50 (2025) e001.
[44] P. Liu, H. Ahmad, B. Mei, et al., Effects of devolatilization temperature on chemical structure and oxidation reactivity of soot sampled from a coflow diffusion ethylene flame, Fuel 293 (2021) 120424.
[45] Y. Ying, D. Liu, Effects of butanol isomers additions on soot nanostructure and reactivity in normal and inverse ethylene diffusion flames, Fuel 205 (2017) 109-29.
[46] I.C. Jaramillo, C.K. Gaddam, R.L. Vander Wal, et al., Effect of nanostructure, oxidative pressure and extent of oxidation on model carbon reactivity, Combust. Flame 162 (2015) 1848-56.
[47] Q.Y. Liu, H.Y. Liu, T.Y. Wang, Numerical study of the effects of surface nitrogen-containing on soot formation process in ammonia/ethylene counterflow diffusion flames, Fuel 383 (2025) 133906.
[48] C. Ao, J. Yan, T. Yan, et al., A theoretical and modeling study of nitrogen chemistry in polycyclic aromatic hydrocarbons growth process, Combust. Flame 259` (2024) 113183.
[49] Y. Zhang, Y. Li, P. Liu, et al., Investigation on the chemical effects of dimethyl ether and ethanol additions

on PAH formation in laminar premixed ethylene flames, Fuel 256 (2019) 115809.
[50] F. Ren, X. Cheng, Z. Gao, et al., Effects of NH3 addition on polycyclic aromatic hydrocarbon and soot formation in C2H4 co-flow diffusion flames, Combust. Flame 241 (2022) 111958.
[51] Y. Yang, S. Zheng, R. Sui, et al., Impact of ammonia addition on soot and NO/N2O formation in methane/air co-flow diffusion flames, Combust. Flame 247 (2023) 112483.
[52] X.B. Cheng, Y. Li, Y.S. Xu, et al., Study of effects of ammonia addition on soot formation characteristics in n-heptane co-flow laminar diffusion flames, Combust. Flame 235 (2022) 111683.
[53] Z. Yan, T. Zhu, X. Xue, et al., Effects of NH3 and H2 addition on morphology, nanostructure and oxidation of soot in n-decane diffusion flames, Fuel Process. Technol. 253 (2024) 108003.
[54] C. Chen, D. Liu, Review of effects of zero-carbon fuel ammonia addition on soot formation in combustion, Renew. Sustain. Energy Rev. 185 (2023) 113640.
[55] M. Zhou, F. Yan, L. Ma et al., Chemical speciation and soot measurements in laminar counterflow diffusion flames of ethylene and ammonia mixtures, Fuel 308 (2022) 122003.
[56] Y. Wang, K. Liu, K. Luo, et al., Study on the mechanism of polycyclic aromatic hydrocarbons and soot formation in ethylene/hydrogen/ammonia laminar diffusion flames, Combust. Flame 277 (2025) 114168.
[57] B. Yang, Z. Yang, J. Wei, et al., Oxidation-induced variations in the physical and fragmentation characteristics of exhaust soot from DMC-diesel blend: Effect of NO presence in the air atmosphere, Fuel 370 (2024) 131817.
[58] V. Volli, A.R.K. Gollakota, C.-M Shu, Comparative studies on thermochemical behavior and kinetics of lignocellulosic biomass residues using TG-FTIR and Py-GC/MS, Sci. Total Environ. 792 (2021) 148392.
[59] S. Liu, H. Yang, K. Zhu, et al., Effect of heavy medium separation on the chemical structure and pyrolysis characteristics of Shenfu coal: insights from FT-IR, XRD, and TG-DTG Analysis, J. Anal. Appl. Pyrolysis 186 (2025) 106975.
[60] J. Yang, H. Chen, W. Zhao, et al., Combustion kinetics and emission characteristics of peat by using TG-FTIR technique, J. Therm. Anal. Calorim. 124 (2016) 519-28.
[61] C. Russo, F. Stanzione, A. Tregrossi, et al., Infrared spectroscopy of some carbon-based materials relevant in combustion: qualitative and quantitative analysis of hydrogen, Carbon 74 (2014) 127-38.
[62] N. Guo, Z. Wang, G. Chen, et al., Co-pyrolysis kinetic characteristics of wheat straw and hydrogen rich plastics based on TG-FTIR and Py-GC/MS, Energy 312 (2024) 133683.
[63] L.Y. Wang, X.X. Cheng, Z.Q. Wang, et al., Effect of the NO plus CO reaction on the consumption of carbon supports: An in situ TG-FTIR analysis, Chem. Eng. J. 352 (2018) 90-102.
[64] X. Gou, X. Zhao, S. Singh, et al., Tri-pyrolysis: A thermo-kinetic characterisation of polyethylene, cornstalk, and anthracite coal using TGA-FTIR analysis, Fuel 252 (2019) 393-402.
[65] B. Tian, Y. Qiao, L. Bai, et al., Management, Pyrolysis behavior and kinetics of the trapped small molecular phase in a lignite, Energy Convers. Manage. 140 (2017) 109-20.
[66] J. Yang, W. Huang, J. Xu, et al., TG-FTIR/MS study on the combustion kinetics and gas emission characteristics of forest duff under different oxygen concentrations, J. Therm. Anal. Calorim. 149 (2024) 9689-702.
[67] L. Wang, C. Song, J. Song, et al., Aliphatic C–H and oxygenated surface functional groups of diesel in-cylinder soot: Characterizations and impact on soot oxidation behavior, Proc. Combust. Inst. 34 (2013) 3099-106.
[68] Y. Liu, S. Wu, C. Fan, et al., Variations in surface functional groups, carbon chemical state and graphitization degree during thermal deactivation of diesel soot particles, J. Environ. Sci. 124 (2023) 678-87.
[69] X. Zhao, J. Wang, J. Li, et al., Kinetic modeling of thermal degradation of TDI/MDI-based flexible polyurethane foam under nitrogen and air atmospheres with Shuffled Complex Evolution algorithm: Insights from TG-FTIR analysis, J. Anal. Appl. Pyrolysis 177 (2024) 106279.
[70] G.C. Lan, J. Li, G.Y. Zhang, et al., Thermal decomposition mechanism study of 3-nitro-1,2,4-triazol-5-one (NTO): Combined TG-FTIR-MS techniques and ReaxFF reactive molecular dynamics simulations, Fuel 295 (2021) 120622.
[71] F. Ren, Z. Li, Y. Fan, et al., Experimental exploration of the N-containing soot precursors in C2H4-NH3 co-flow diffusion flames, Combust. Flame 276 (2025) 114104.
[72] C. Fan, Z. Guan, J. Wei, et al., An assessment of soot chemical property from a modern diesel engine fueled with dimethyl carbonate-diesel blends, Fuel 309 (2022) 122220.
[73] Z.Y. Zhang, K.L. Kang, L.H. Li, et al., Characterization of moxa floss combustion by TG/DSC, TG-FTIR and IR, Bioresour. Technol. 288 (2019) 121516.
[74] C. Shao, F. Campuzano, Y. Zhai, et al., Effects of ammonia addition on soot formation in ethylene laminar premixed flames, Combust. Flame 235 (2022) 111698.
[75] M. Asemani, A.R. Rabbani, Detailed FTIR spectroscopy characterization of crude oil extracted asphaltenes: Curve resolve of overlapping bands, J. Pet. Sci. Eng. 185 (2020) 106618.
[76] J. Winiarski, W. Tylus, K. Winiarska, et al., XPS and FT-IR Characterization of Selected Synthetic Corrosion Products of Zinc Expected in Neutral Environment Containing Chloride Ions, J. Spectrosc. 203 (2018) 2079278..
[77] Y. Liu, C. Song, G. Lv, et al., Surface functional groups and sp3/sp2 hybridization ratios of in-cylinder soot from a diesel engine fueled with n-heptane and n-heptane/toluene, Fuel 179 (2016) 108-13.
[78] A. Zygogianni, M. Syrigou, A.G. Konstandopoulos, et al., Oxidative reactivity of particulate samples from different diesel combustion systems and its relation to structural and spectral characteristics of soot, Emiss. Control Sci. Technol. 5 (2019) 99-123.
[79] C. Fan, J. Wei, H. Huang, et al., Chemical feature of the soot emissions from a diesel engine fueled with

methanol-diesel blends, Fuel 297 (2021) 120739.
[80] G.D.G. Peña, M.M. Alrefaai, S.Y. Yang, et al., Effects of methyl group on aromatic hydrocarbons on the nanostructures and oxidative reactivity of combustion-generated soot, Combust. Flame 172 (2016) 1-12.
[81] B. Azambre, S. Collura, J.M. Trichard, et al., Nature and thermal stability of adsorbed intermediates formed during the reaction of diesel soot with nitrogen dioxide, Appl. Surf. Sci. 253 (2006) 2296-303.
[82] O.B. Popovicheva, E.D. Kireeva, N.K. Shonija, et al., FTIR analysis of surface functionalities on particulate matter produced by off-road diesel engines operating on diesel and biofuel, Environ. Sci. Pollut. Res. Int. 22 (2015) 4534-44.
[83] G. Karavalakis, V. Boutsika, S. Stournas, et al., Bio-diesel emissions profile in modern diesel vehicles. Part 2: Effect of biodiesel origin on carbonyl, PAH, nitro-PAH and oxy-PAH emissions, Sci. Total Environ. 409 (2011) 738-47.
[84] A. Macor, F. Avella, D.J.A.E. Faedo, Effects of 30% v/v biodiesel/diesel fuel blend on regulated and unregulated pollutant emissions from diesel engines, Appl. Energy 88 (2011) 4989-5001.
[85] P.E. Fanning, M.A. Vannice, A DRIFTS study of the formation of surface groups on carbon by oxidation, Carbon 31 (1993) 721-30.
[86] M.H. Zaher, M. Dadsetan, C. Chu, et al., The effect of ammonia addition on soot nanostructure and composition in ethylene laminar flames, Combust. Flame 251 (2023) 112687.
[87] A. Tapia, S. Salgado, P. Martín, et al., Chemical composition and heterogeneous reactivity of soot generated in the combustion of diesel and GTL (Gas-to-Liquid) fuels and amorphous carbon Printex U with NO2 and CF3COOH gases, Atmos. Environ. 177 (2018) 214-21.

Table 1

Flow rate conditions for the present laminar diffusion flame.

case	C_2H_2 flow rate/(mL·min^{-1})	NH_3 flow rate/(mL·min^{-1})	N_2 flow rate/(mL·min^{-1})	Air flow rate/(L·min^{-1})	X_{NH_3}/%
N_{00}	200	0	300	20	0
N_{20}	200	100	200	20	20
N_{40}	200	200	100	20	40
N_{60}	200	300	0	20	60

Table 2

Oxidation kinetic parameters of soot from different X_{NH_3}.

condition	T_i/℃	T_{max}/℃	T_e/℃	Peak oxidation rate/mg·s^{-1}	E_a/kJ·mol^{-1}	R^2
N_{00}	520	594	620	12.9×10^{-3}	142.5	0.96
N_{20}	507	559	591	14.6×10^{-3}	124.9	0.95
N_{40}	506	557	576	14.7×10^{-3}	122.5	0.99
N_{60}	497	553	575	14.9×10^{-3}	114.1	0.97

Figure 1

Click here to access/download;Figure;Fig. 1.jpg

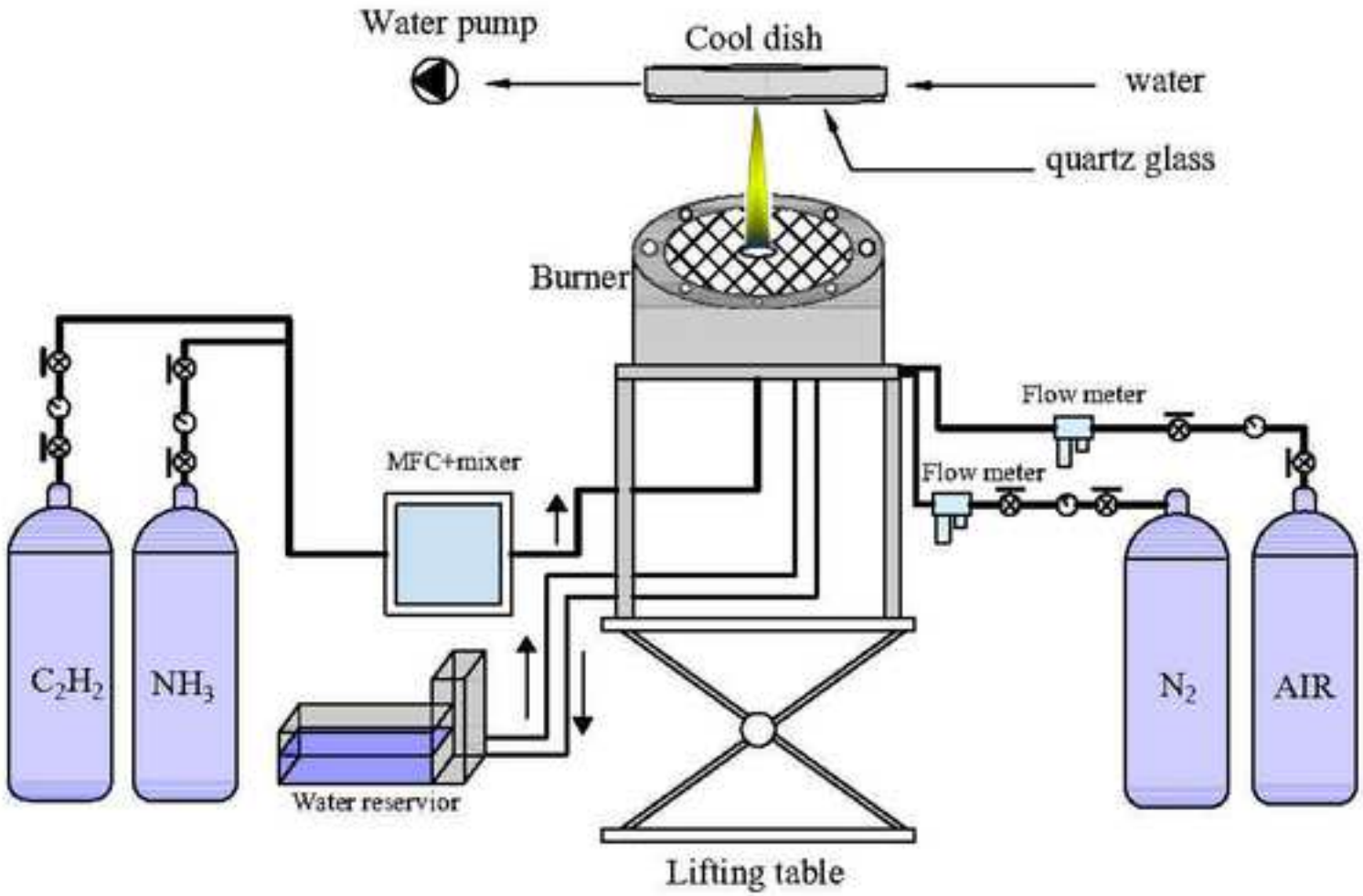

Figure 2

Click here to access/download;Figure;Fig. 2.jpg

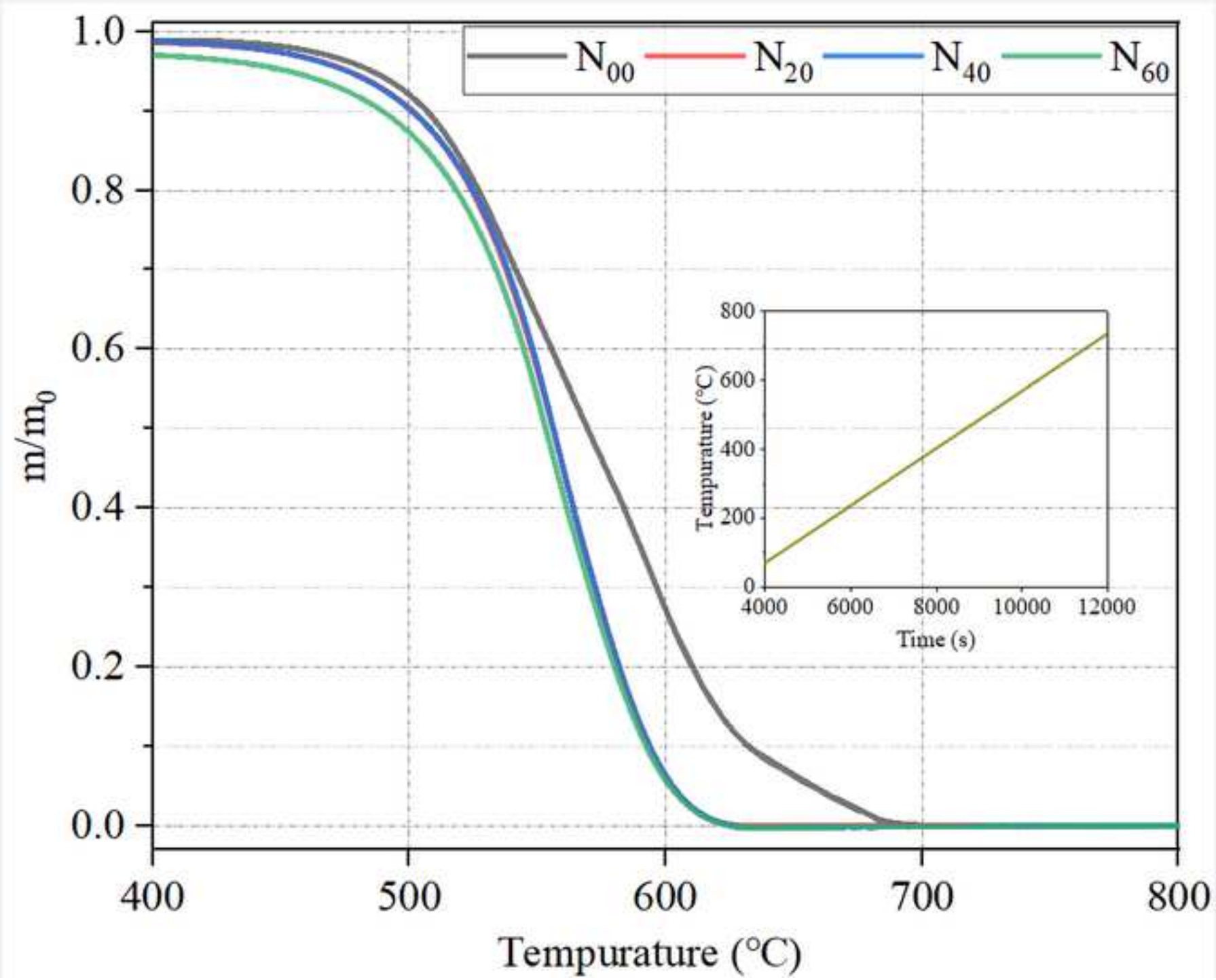

Figure 3

Click here to access/download;Figure;Fig. 3.tif

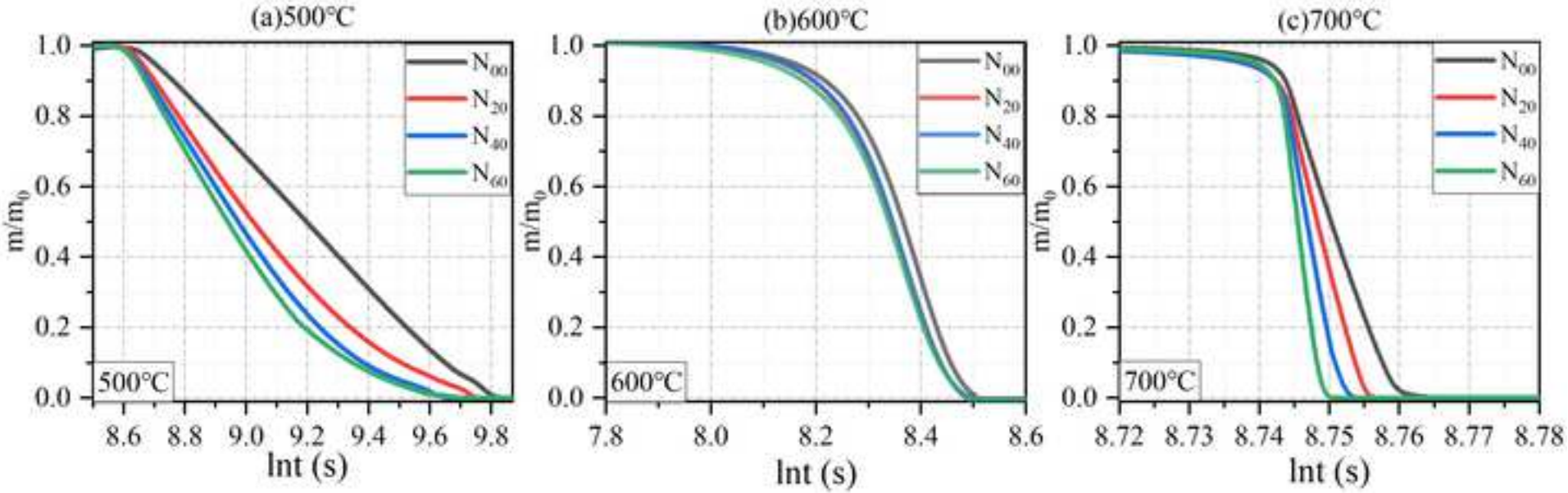

Figure 4

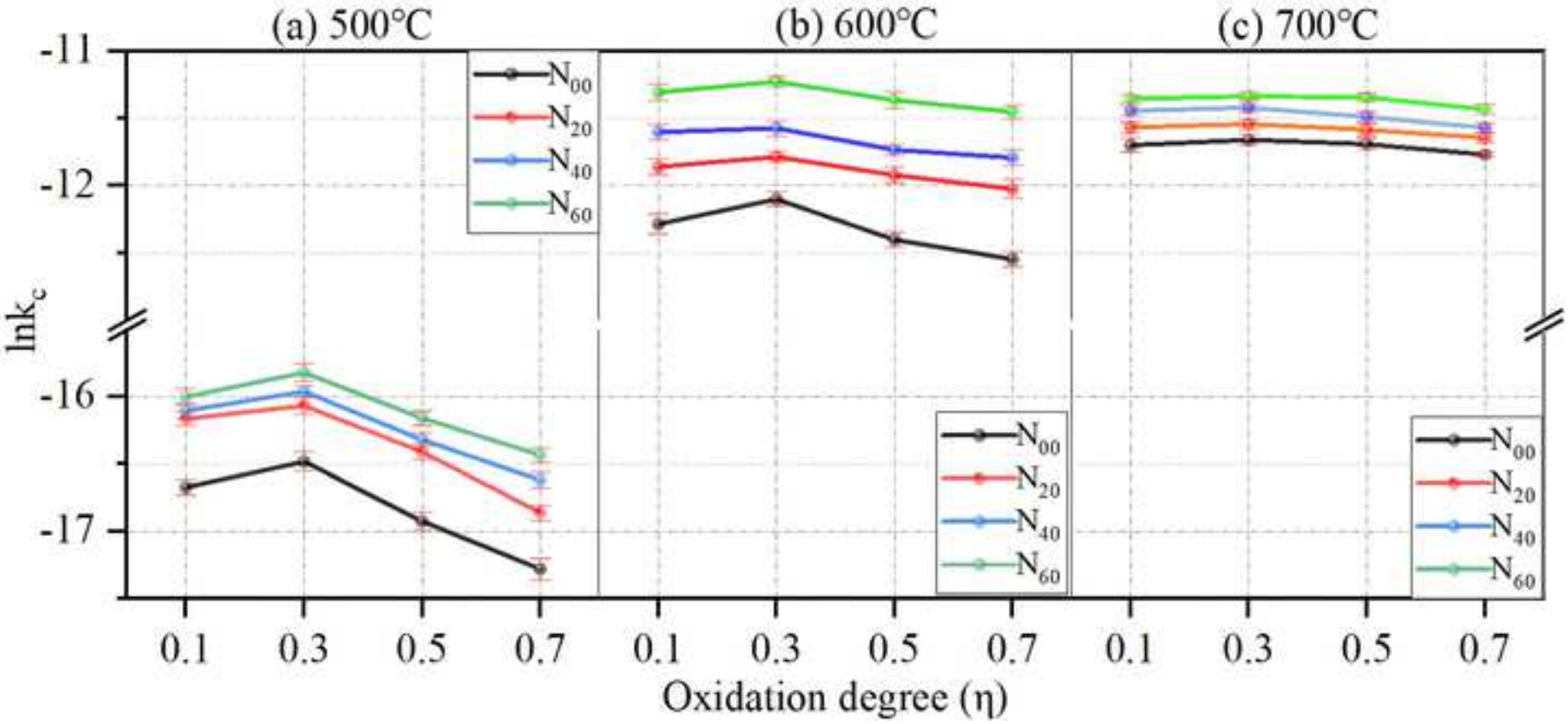

Figure 5

Click here to access/download;Figure;Fig. 5.jpg

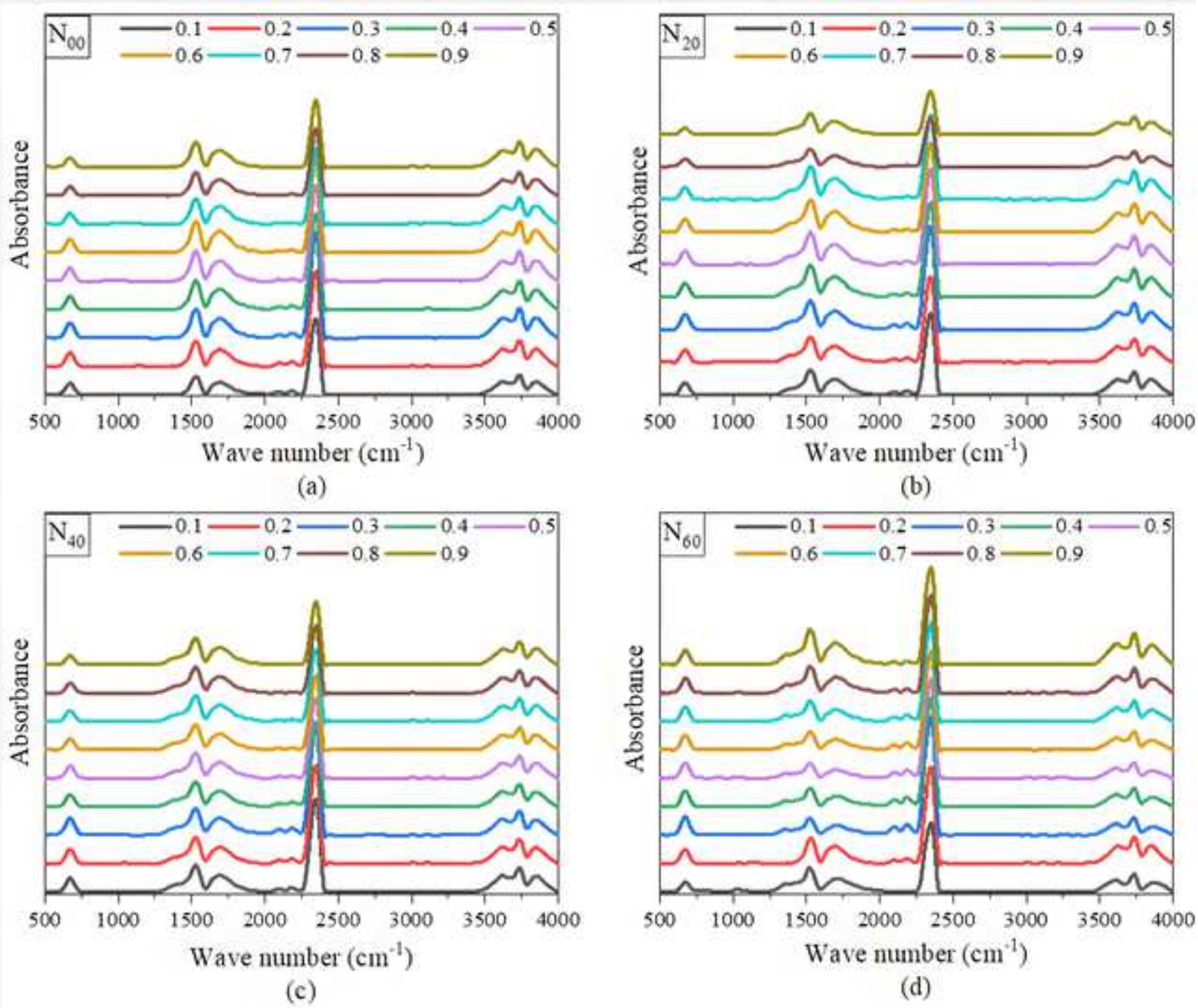

Figure 6

Click here to access/download;Figure;Fig. 6.jpg

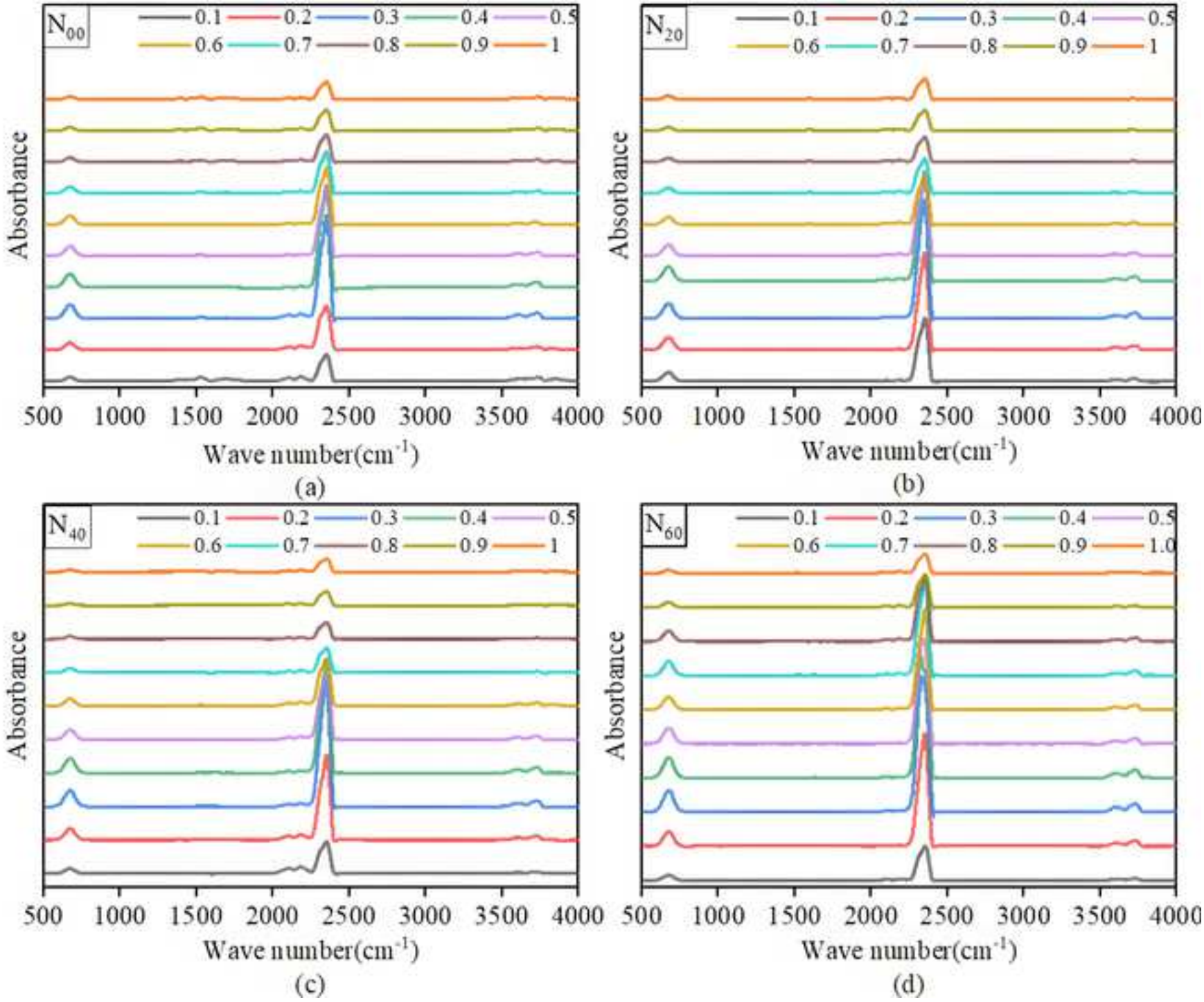

Figure 7

Click here to access/download;Figure;Fig. 7.tif

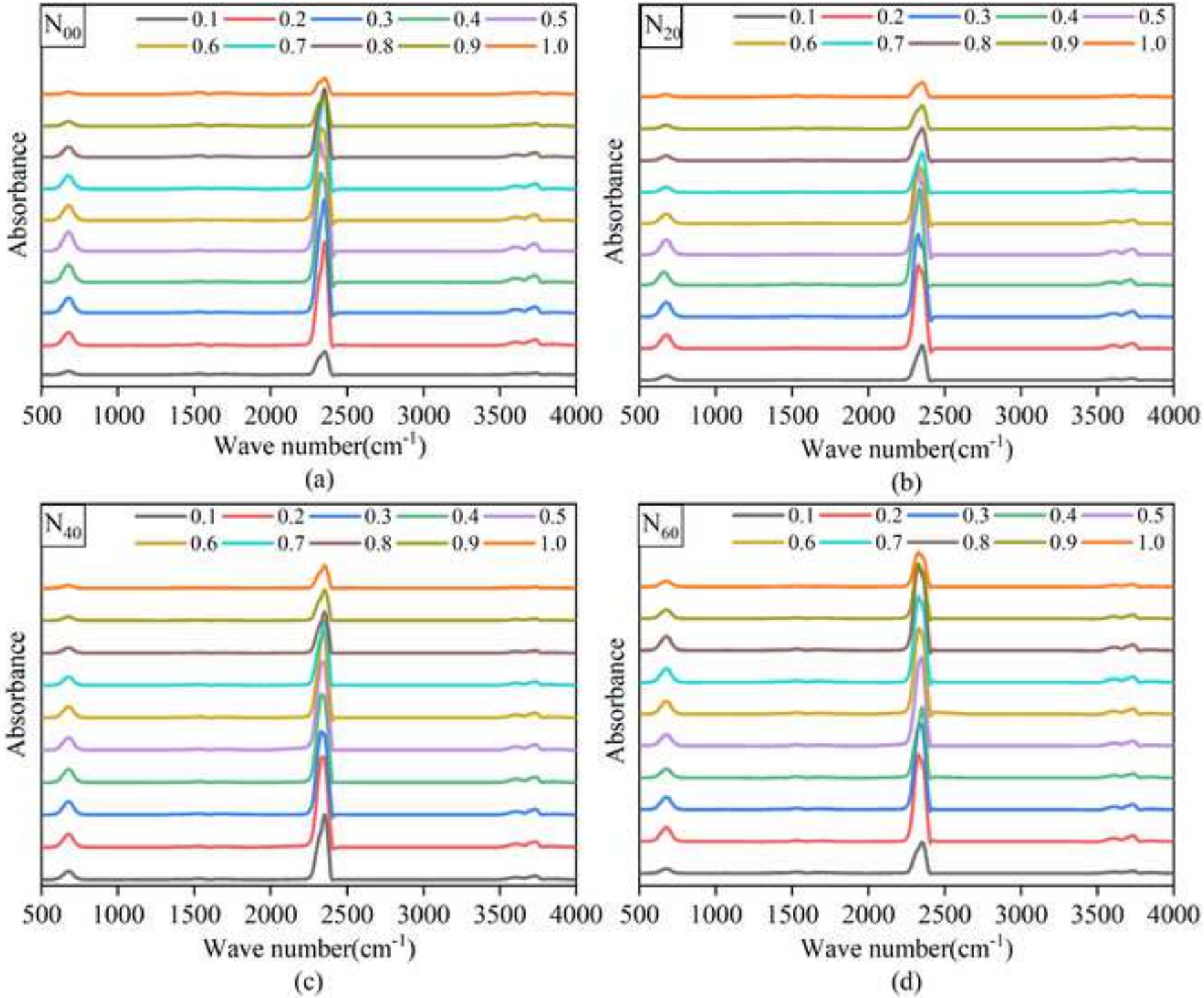

Figure 8

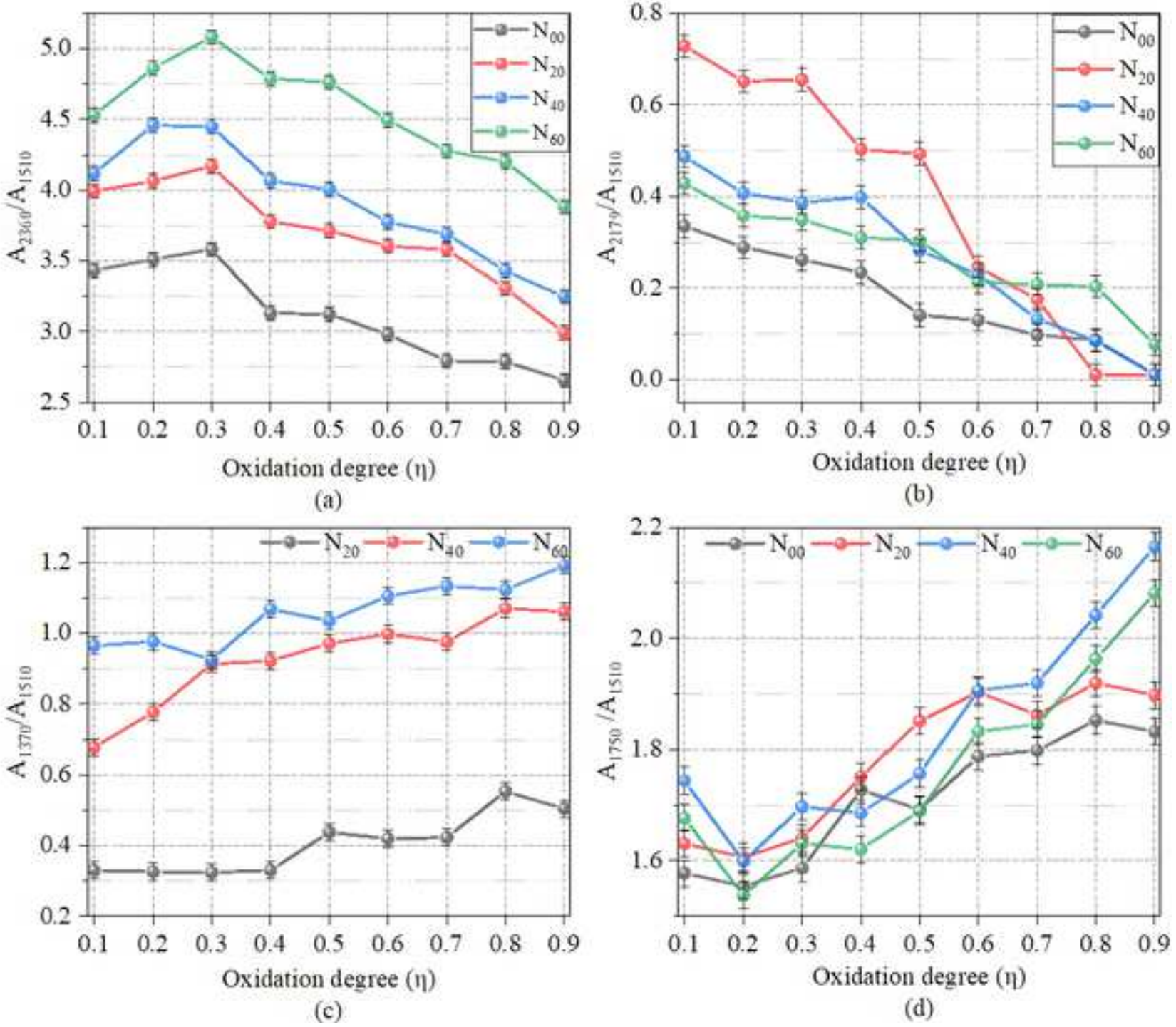

Figure 9

Click here to access/download;Figure;Fig. 9.jpg

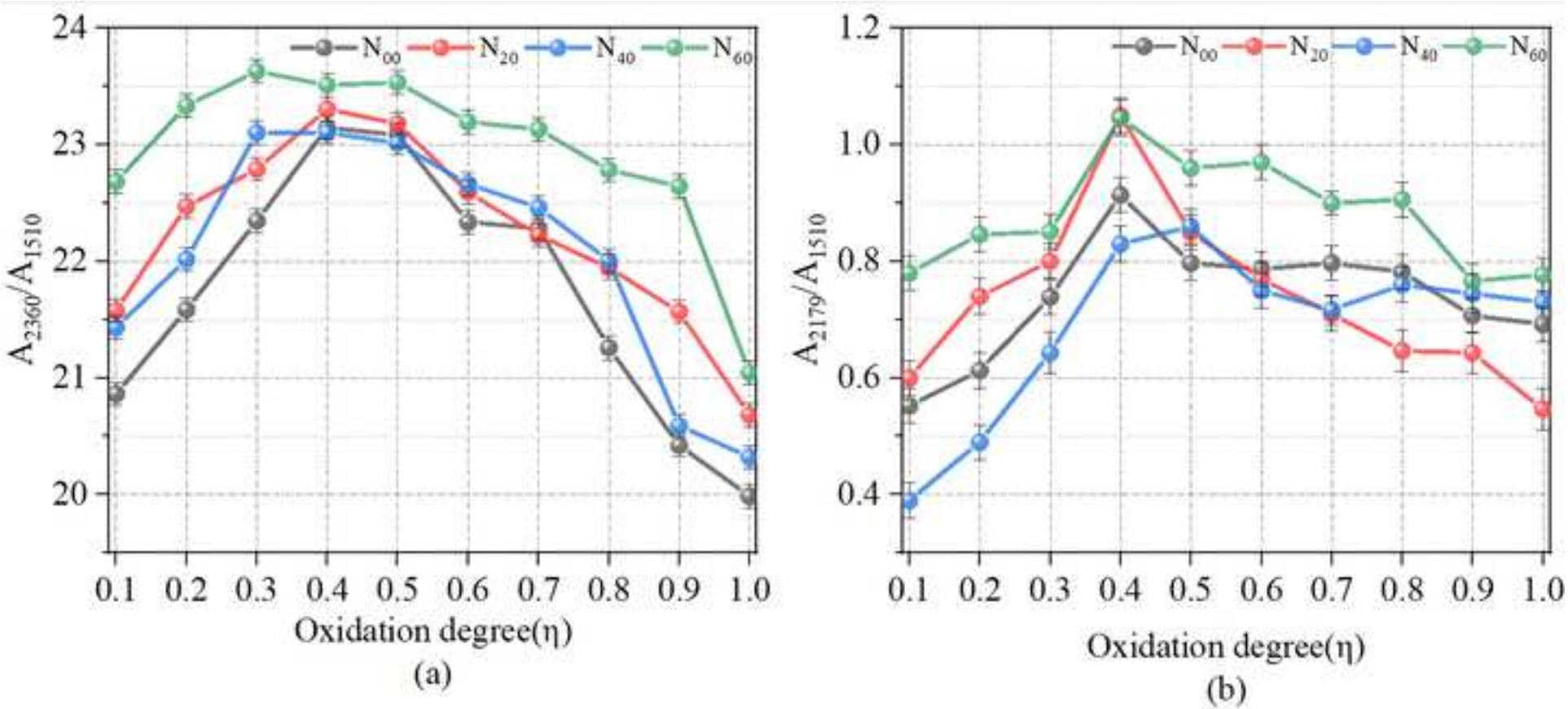

Figure 10

Click here to access/download;Figure;Fig. 10.jpg

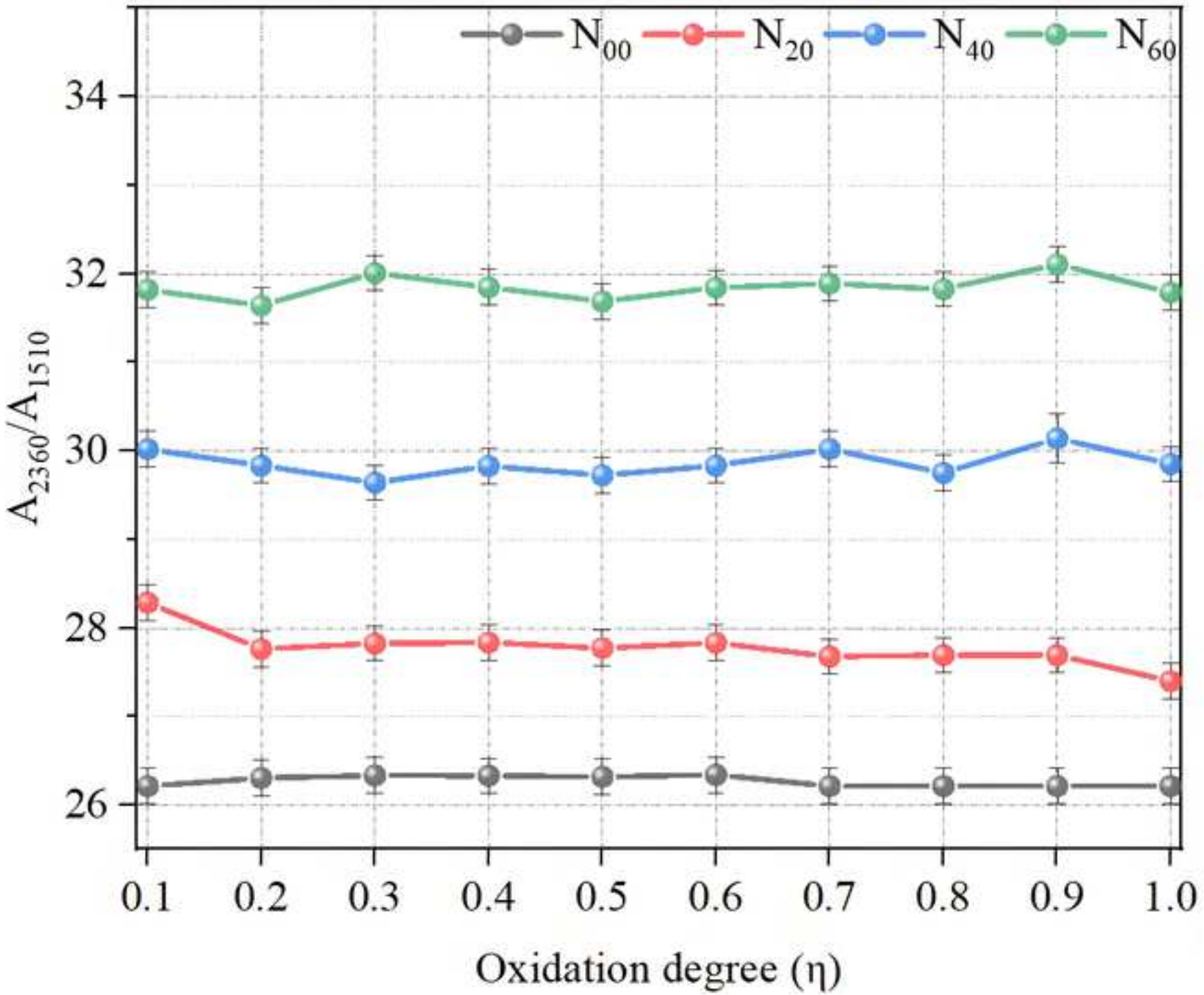

Figure 11

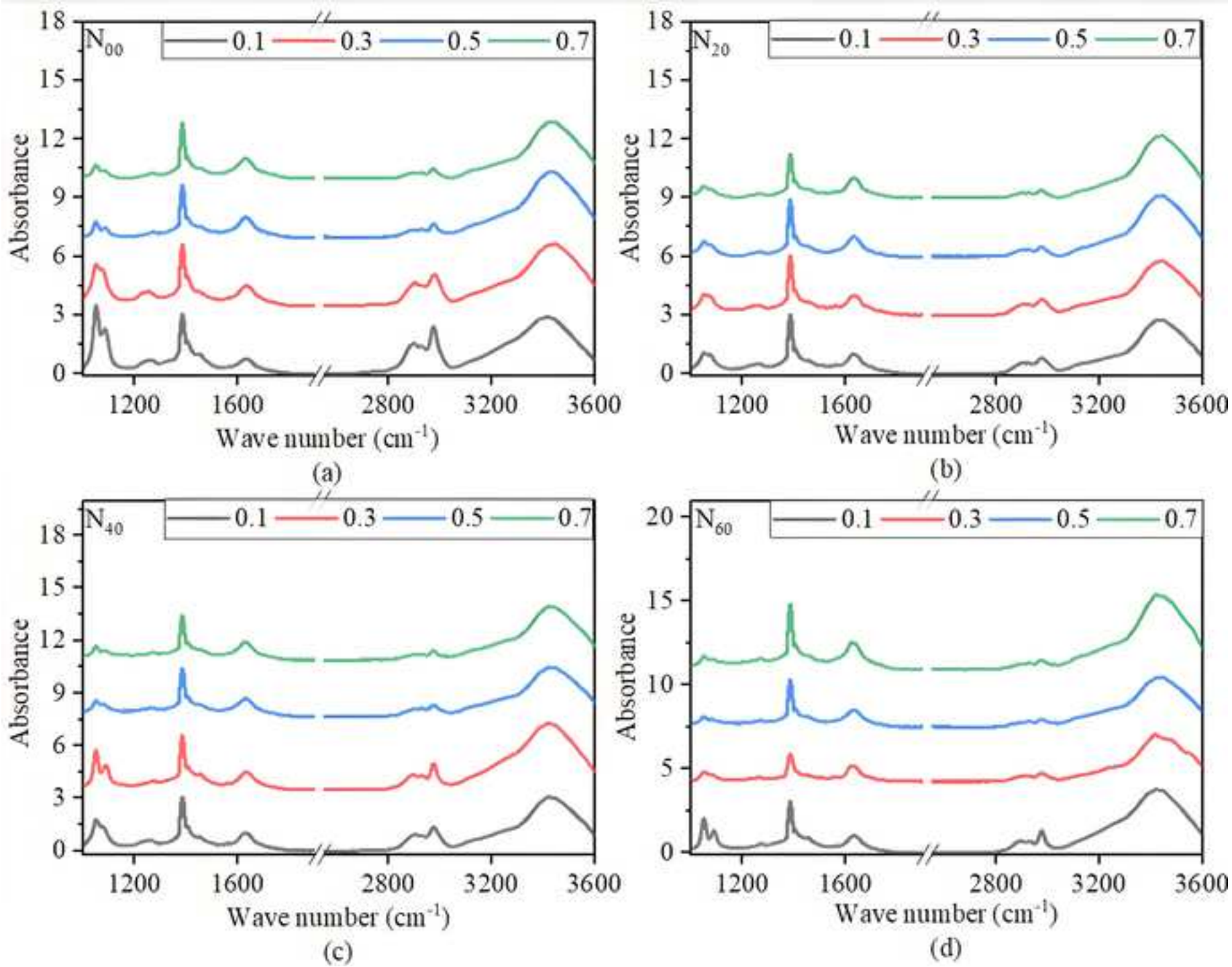

Figure

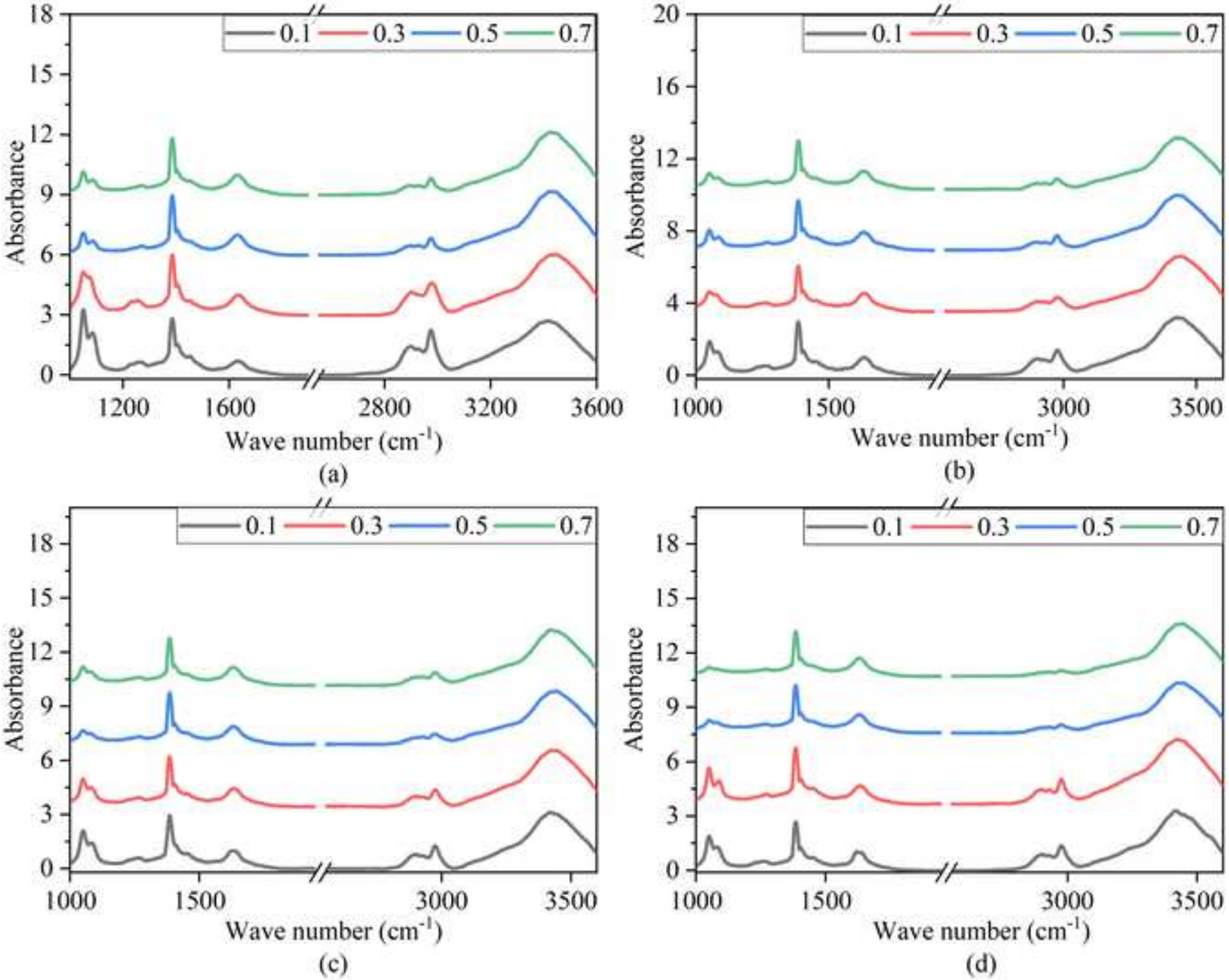

Figure 13

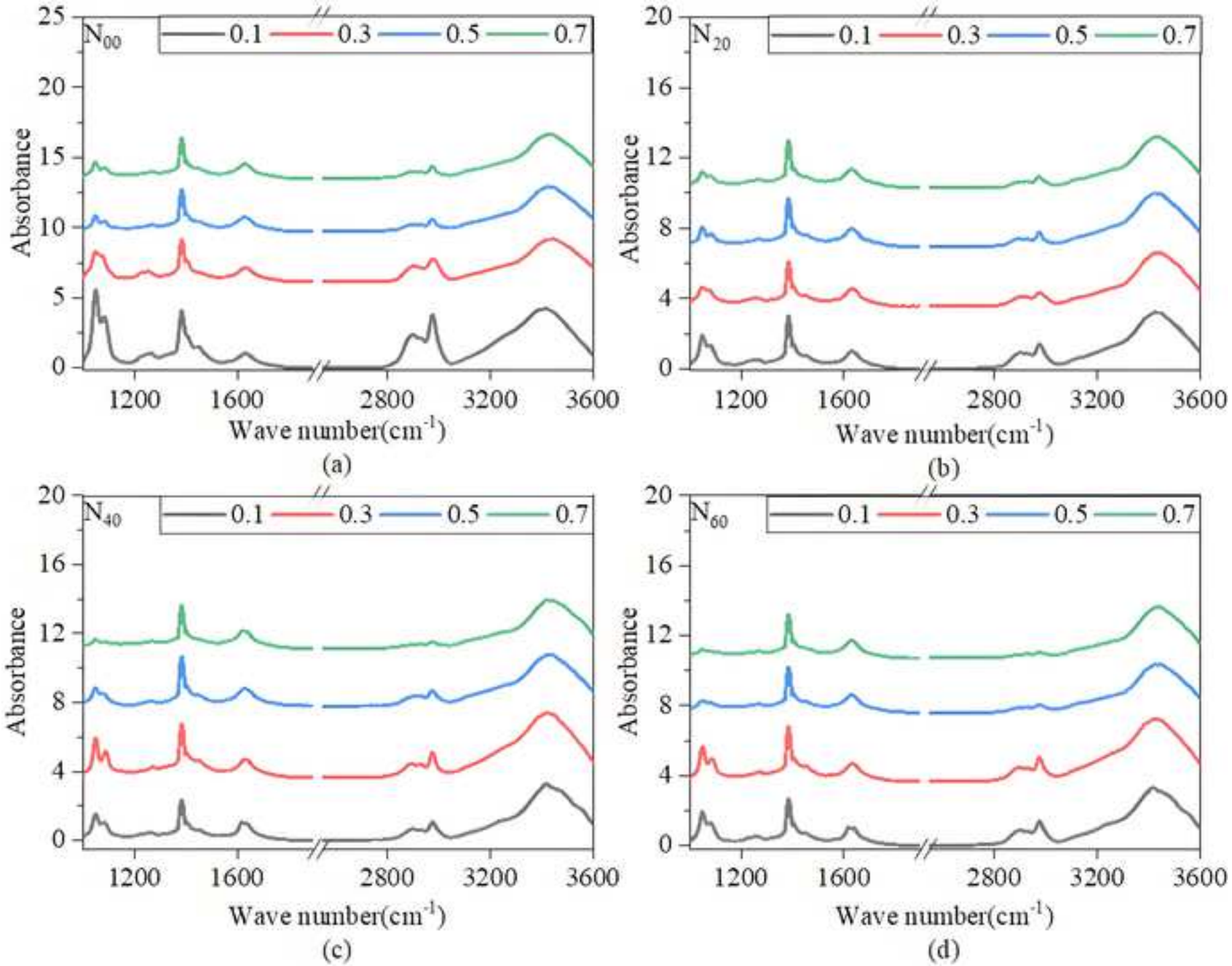

Figure 14

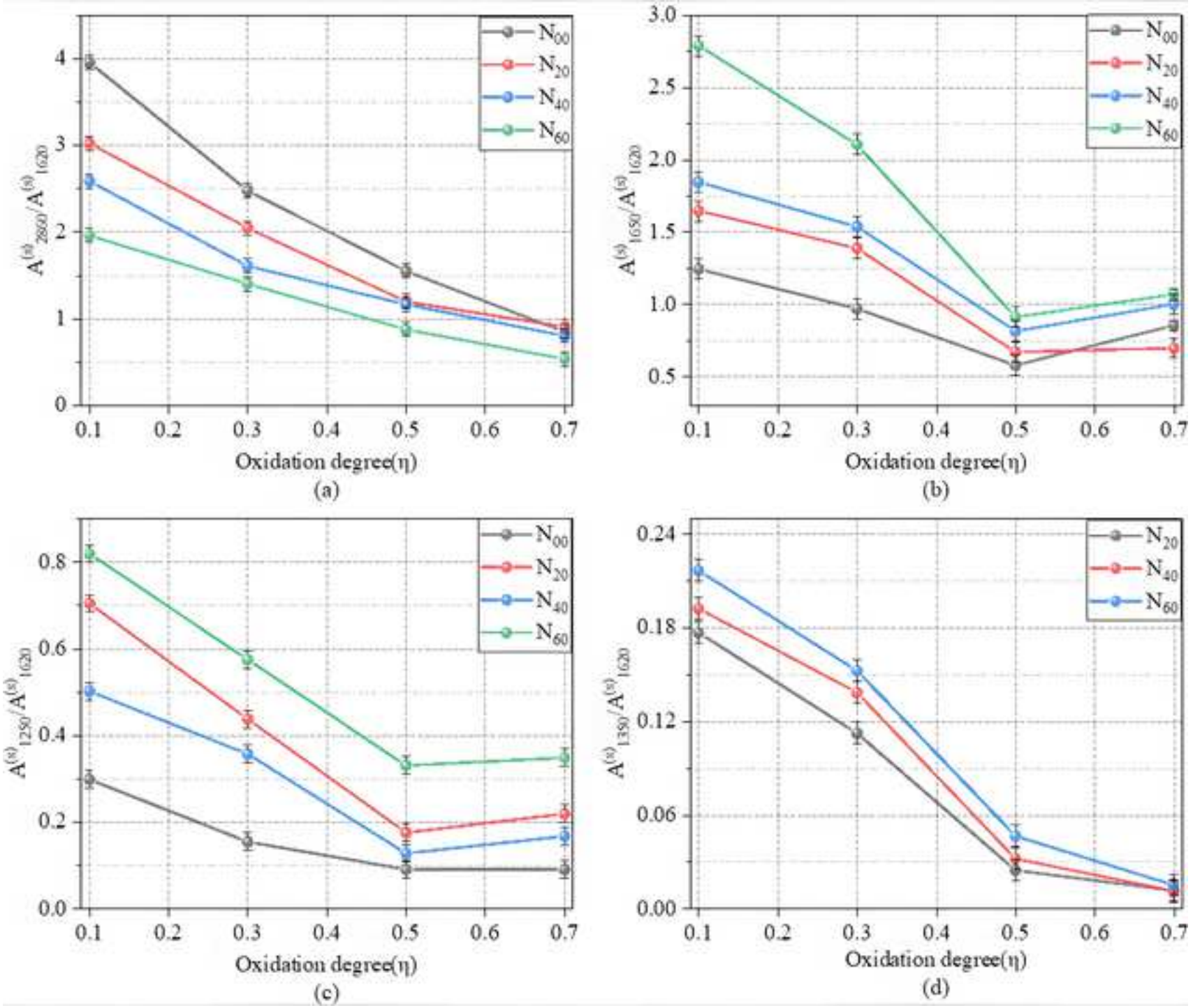

Figure 15

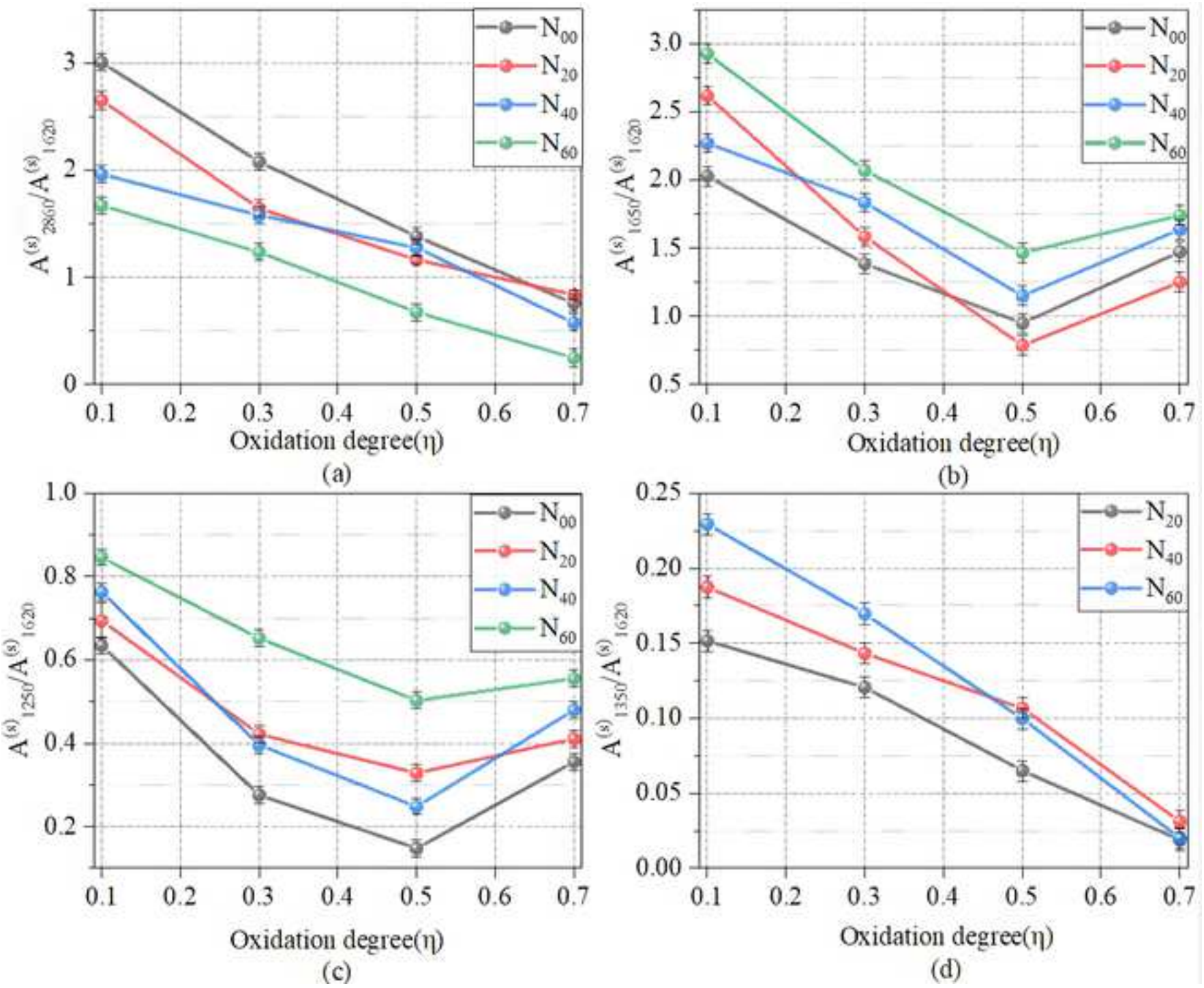

Figure 16

Click here to access/download;Figure;Fig. 16.jpg